1   **Can multi-scale thermal infrared imaging help validate and monitor water stress in**

2   **alluvial forests?**

3

4   Authors : J. Godfroy[1,2*], P. Malherbe[1], F. Gerle[3], B. Marteau[1,4], P. Lochin[1], S. Puijalon[3], J.

5   Lejot[5], A. Vernay[3], H. Piégay[1]

6   [1] Univ of Lyon, ENS Lyon, CNRS, UMR 5600 EVS, F-69342 Lyon, France ;

7   pauline1malherbe@gmail.com ; pierre.lochin@ens-lyon.fr ; herve.piegay@ens-lyon.fr

8   [2] Now at : Univ. Grenoble Alpes, INRAE, LESSEM, F-38402 St-Martind'Hères, France ;

9   julien.godfroy@inrae.fr

10   [3] Univ of Lyon, Université Claude Bernard Lyon 1, LEHNA UMR 5023, CNRS, ENTPE, F-

11   69622 Villeurbanne, France ; flavie.gerle@orange.fr ; sara.puijalon@univ-lyon1.fr ;

12   antoine.vernay@univ-lyon1.fr

13   [4] Now at : Univ Rennes 2, UMR6554 LETG, F-35043 Rennes, France ;

14   baptiste.marteau@univ-rennes2.fr

15   [5] Univ of Lyon, Univ. Lumière Lyon 2, CNRS, UMR 5600 EVS, F69342 Lyon, France ;

16   jerome.lejot@univ-lyon2.fr

17   [*] Corresponding author : julien.godfroy@inrae.fr

18

24

Abstract.

Alluvial forests are fragile and sensitive to drought induced by climate change and exacerbated by altered flow regimes. Our ability to detect and map their sensitivity to drought is therefore crucial to evaluate the effects of climate change and adjust management practices. In such a context, we explore the potential of multi-scale thermal infrared imagery (TIR) to diagnose the sensitivity of alluvial forests to drought events. In summer 2022, we sampled leaves and phloem on *Populus nigra* trees from two sites with contrasted hydrological connectivity along the Ain River (France) in order to investigate the seasonality of water stress and act as ground truth for airborne TIR images. To map forest sensitivity to drought, we then used a set of TIR data from four existing airborne campaigns and Landsat archives over a larger spatial and temporal extent. Field data showed that stress conditions were reached for both sites during summer but were higher in the site with lower groundwater connectivity, which was also the case for individual tree crown temperature. At the forest plot scale, canopy temperature was linked to forest connectivity for two of four airborne TIR campaigns, with higher values in the more degraded reaches. The data from the Landsat archives at the landscape scale was used to locate the areas of the riparian forest impacted by a historical drought event, and monitor their recovery. TIR data showed promising results to help detect and map tree water stress in riparian environments. However, stress is not detected in all TIR campaigns, demonstrating that in-field ecophysiological measurements are complementary to validate observations and one-shot acquisitions are not enough to diagnose stress. More integrative indicators of drought stress are needed at a seasonal scale, one-shot acquisitions on a given day can inform potential heat disturbance effects but do not really give information on the cumulative effects of heat pulses over the whole vegetative season (ramp-disturbance effect). Landsat data was useful to identify trends but may be less representative

49 of stress due to coarse spatial resolution and potential confounding factors related to changes

50 in successional stages (tree height and density...) at larger temporal scales.

51

52 **Key words.**

53 Riparian Vegetation, Water Stress, Thermal Infrared Remote Sensing, Multi-method

54 Approach, Anthropogenic Alterations

55

56 **1. Introduction.**

57 Alluvial forests are unique environments characterized by complex feedback processes with

58 their river system that provide a set of ecosystem services (Naiman et al., 1988; Riis et al.,

59 2020). Alluvial forests are biodiversity hotspots (Naiman et al., 1993), improve water quality

60 (Dosskey et al., 2010; Tabacchi et al., 2000), help stabilize channel banks (Simon and

61 Collison, 2002) and play a key role in ensuring the sustainability of good hydromophological

62 conditions in river systems (González del Tánago et al., 2021).

63 Human development in the 20th century has however caused increased pressure on riparian

64 vegetation (Bravard et al., 1997; Breton et al., 2023; Comiti et al., 2011; Poff et al., 2007).

65 Activities such as gravel mining, damming and engineering works have induced tree stress

66 and increased mortality (Scott et al., 2000), and led to a reduction of forest renewal by

67 increasing bank resistance or reducing channel mobility in other cases (Décamps et al., 1988;

68 Dépret et al., 2023). Key riparian species are also sensitive to climate change (O'Briain,

69 2019). Higher temperatures and variations in precipitations and flow regimes brought about

70 by climate change can impact tree water use and water availability (Rivaes et al., 2013; Stella

71 et al., 2013b). Groundwater decline due to drought or anthropogenic alterations can induce

stress and higher mortality in riparian woodlands, and lead to long-term shifts in species composition (Breton et al., 2023; Janssen et al., 2020; Kibler et al., 2021; Rohde et al., 2021). Therefore, it is important to monitor the response of riparian vegetation to events affecting water availability such as channel incision due to damming or mining and droughts due to climate change. Such a monitoring effort can then help target conservation and restoration actions to mitigate negative impacts of global change on riparian forests and assess their efficiency.

Field surveys are traditionally used to assess the water status of individual trees. For example, tree rings can give insights into events happening within the lifespan of an individual and radial growth anomalies can occur during dryer years (Dufour and Piégay, 2008; Singer et al., 2013; Stella et al., 2013a). Other less destructive methods such as sampling tree leaves or phloem can also inform about tree water status. The measure of leaf water potential (LWP) can indicate on-going water stress of the tree at the time of sampling (Brodribb and Holbrook, 2003; Scholander et al., 1965). Carbon isotope analysis of the phloem content can help determine how efficient a tree is at using water to produce biomass (intrinsic Water Use Efficiency, iWUE), which responds to water deficits such as drought-related stress (Klein et al., 2016; Seibt et al., 2008). One of the main limitations of such approaches however is that they are time-intensive and cannot easily be conducted at a large scale within a short time window.

At the scale of communities or river reaches, remote-sensing has been used to assess forest status with imagery in the visible and near infrared spectrum (Kibler et al., 2021), or in the thermal infrared (TIR) spectrum (Mayes et al., 2020). In these cases, TIR data is used since differences in canopy temperatures are a good indicator of differences in evapotranspiration. Even though remote sensing applications are increasingly common to study riparian

96   vegetation, the use of TIR sensors has been mostly limited to the use of satellite-based sensors

97   in arid or semi-arid climates where drought events are common today [Table 1].

98   **Table 1. - Examples of recent thermal infrared studies focusing on riparian vegetation.**

Study	Sensor	Vector	Objective	Climate	Time Series
(Neale et al., 2011)	FLIR SC640	Aircraft	Estimating evapo-transpiration	Mediterranean (California)	
(Gokool et al., 2017)	MODIS + Landsat	Satellite	Retrieving daily evapo-transpiration from satellite data	Semi-Arid (South Africa)	X
(Fairfax and Small, 2018)	Landsat	Satellite	Assessing the impact of beaver damming on evapo-transpiration	Arid (Nevada)	X
(Lurtz et al., 2020)	Landsat	Satellite	Relationship between evapo-transpiration and modeled water table depths	Semi-Arid (Colorado)	X
(Ciężkowski et al., 2020)	Landsat	Satellite	Comparing thermal and optical indexes to detect stress	Temperate transitional (Poland)	X
(Mayes et al., 2020)	Landsat	Satellite	Understanding water use at landscape scale	Semi-Arid (Mexico)	X
(Sankey et al., 2021)	SenseFly thermoMAP	UAV	Detecting genetic traits differences	Semi-Arid (Central Arizona)	

99

One of the advantages of using data from satellites is that they can cover large spatial scales at a temporal resolution that cannot be matched by airborne surveys (*e.g.* 8-day repeat coverage for Landsat data and near daily coverage for MODIS data). This enables monitoring the impact of specific climate events by investigating the consequences of drought or changes in groundwater accessibility on water use by riparian trees (Lurtz et al., 2020; Mayes et al., 2020). A key disadvantage of satellite data however, is that spatial resolution is coarse for spectral bands in the TIR region, for instance with 100 meters at-sensor resolution for Landsat 8 and 9 which is then resampled afterwards to fit the 30 meters resolution of Landsat products.

Finer spatial resolution is available when mounting TIR sensors on airborne vectors such as an airplane or a UAV and can also be used to assess the health status of the vegetation or evapo-transpiration (Neale et al., 2011). A recent study showed that it was possible to detect genetic traits differences between cottonwood trees from different populations planted in the same plantation (Sankey et al., 2021). This suggests that airborne TIR imagery can also provide critical insights into riparian vegetation, but studies using such vectors are rare.

Additionally, for aircraft acquisitions that can provide the combination of spatial extent and resolution which is the most interesting to stakeholders, acquiring repeated observations over an entire phenological seasons is usually difficult. While airborne TIR images are not often used to assess vegetation health, acquisitions over river corridors are already frequent and have led to multiple publications focusing on the surface temperature of rivers (see for instance a guide aimed at practitioners (Dugdale, 2016)). Indeed, knowledge of river temperature helps target areas of ecological interest for species living in the river and helps conservation efforts. Thermal refuges are of increasingly high importance for species in

120 warming waters (Dugdale et al., 2016; Wilbur et al., 2020), and monitoring the thermal

121 functioning of rivers provides insights to assess the impact of restoration projects (Marteau et

122 al., 2022a). Data acquired for such studies also covers riparian vegetation but usually only

123 focuses on the shading effects provided by trees and on their ability to lower water

124 temperature during summer (Dugdale et al., 2018; Marteau et al., 2022b; Wawrzyniak et al.,

125 2017; Whitledge et al., 2006).

126 Therefore, thermal infrared data is available from either satellite or airborne sensors with

127 promising potential to provide feedback about riparian vegetation health but this potential has

128 yet to be assessed and confronted to in-field eco-physiological measurements of water stress

129 in the riparian environment.

130 In this context, this study aims at exploring the potential of multi-scale thermal infrared data

131 to diagnose the sensitivity of riparian forests to drought events.

132 To address those aims, we (1) tested the validity of TIR information as a good indicator of

133 water stress by coupling field evidence from ecophysiological surveys conducted at an

134 individual scale during summer 2022 with a simultaneous TIR acquisition during the peak of

135 the drought period. This enabled (2) the comparison of 4 existing historical airborne TIR

136 acquisitions to study the response sensitivity of the forest to a set of potential drought events

137 over a 50 km reach and then (3) the replication of a similar temporal analysis using TIR

138 satellite data in order to identify lasting changes at the corridor scale over a longer time scale

139 (*e.g.*, 34 years).

140 Our chosen study site was the riparian corridor of the Ain River because (1) it is large enough

141 to be approached using Landsat imagery, (2) airborne TIR images have historically been

142 acquired over the corridor to study river temperature, and (3) the forest is dominated by the

143 phreatophyte *Populus nigra* populations established on sites with contrasting connectivity to

144 the river.

145

146 **2. Study Site.**

147 The Ain River is one of the main tributaries of the upper Rhône River in France. During the

148 20th century, a chain of dams was built on this large, meandering gravel-bed river for

149 hydroelectric purposes, causing a sediment starvation that propagates downstream by 500

150 meters per year on average and results in a channel incision of 1 to 2 meters (Rollet, 2007;

151 Rollet et al., 2014). We focus on a 50-km long reach that starts downstream of this chain of

152 dams and ends at the confluence with the Rhône River, which is referred to as the lower Ain

153 River valley [Figure 1]. The upstream section of the lower Ain River (R1) is characterized by

154 sediment starvation and channel incision induced by the upstream dams. Downstream from

155 this incised reach, elevation of the riverbed is stable and active channel meandering occurs

156 and rejuvenates the riparian forest (R2). Further downstream is another reach affected by

157 sediment starvation because of the combined effects of sediment trapping in R2 and limited

158 local production due to lateral constraints by morainic deposits (R3). Finally, the reach of the

159 river that leads to its confluence with the Rhône River has been historically affected by

160 regressive incision from the Rhône River but now produces enough sediment due to channel

161 meandering to lead to aggradation near the confluence in recent years (R4).
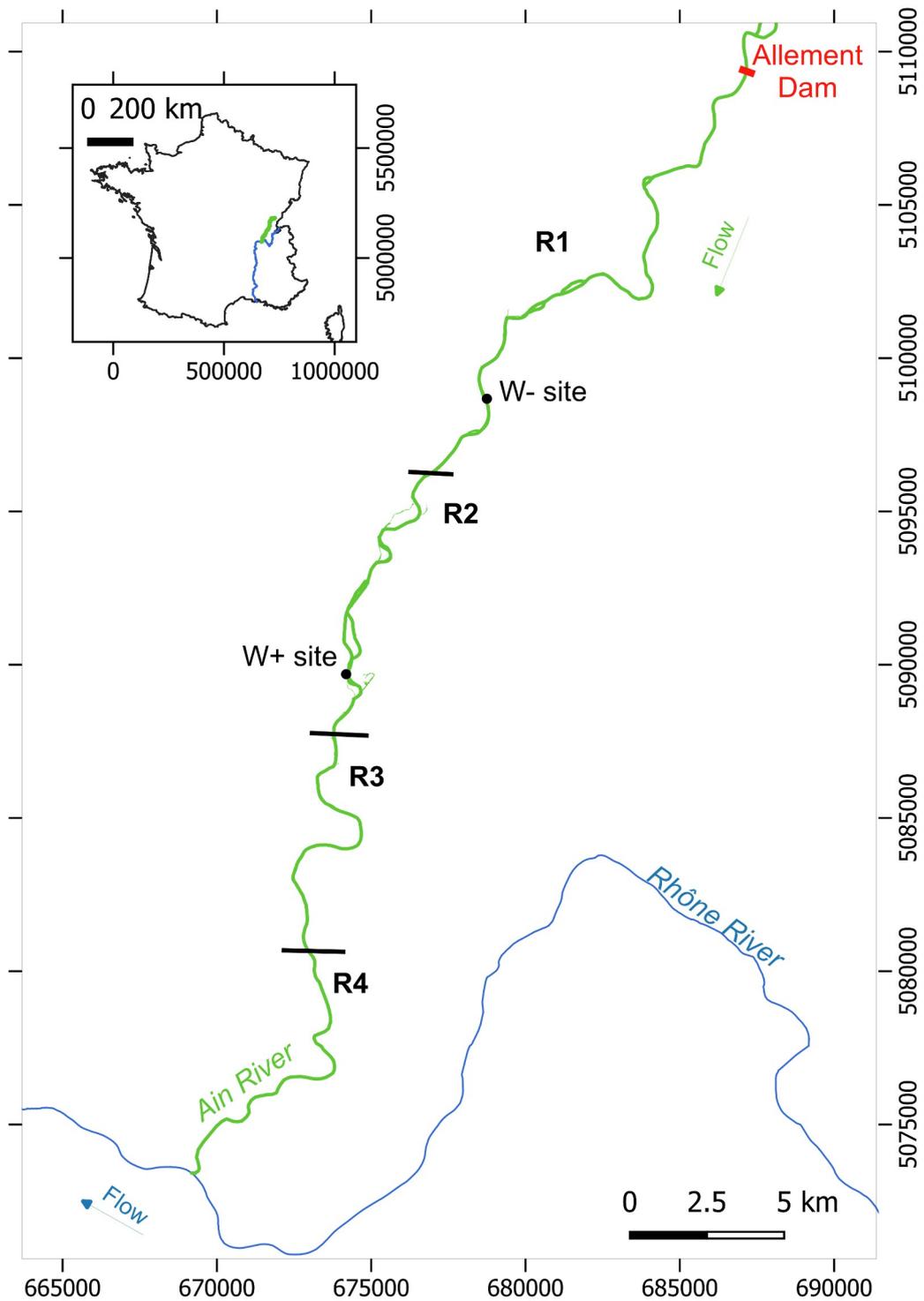
Figure 1. - Location of the lower Ain River and of the different study reaches. The coordinate system is EPSG 2154.

Traditional on-field forestry surveys conducted in 2008 and 2017 by the French National Forestry Office (ONF) (Dumas, 2017; Dumas and Perrin, 2006) showed that the dominant

9

species in the riparian forest is *Populus nigra.* These studies also suggested that sediment starvation and channel incision have an impact on the health of the riparian forest along the Ain River, with a relative loss of native pioneer species (*Populus nigra*, *Salix alba*, *Salix eleagnos*) in favour of exotic (*Fallopia japonica*) or post-pioneer (*Fraxinus excelsior*) species. They also mention high mortality of poplar trees in the sector near the confluence that they attribute to drought events in the early 2000s.

This degraded health status of the riparian forest is visible as a downward trend in NDVI from Landsat images (Lejot et al., 2011) as well as from a study looking at the long-term impacts of channel incision by coupling the data from the ONF field surveys with LiDAR and hyperspectral datasets (Godfroy et al., 2023). This later study highlighted that in reach R1, the relative elevation of the riparian forest from the base flow waterline is higher than in reach R2 which results in an increased distance to the groundwater table and a dryer environment. The Ain River is therefore an interesting site to address our aims because the known changes in forest composition, structure, and reflectance in the visible and near-infrared spectrum based on forest stationary conditions suggests that water stress occurs during the growing period and that some poplar trees are known to have responded to a dryer environment.

3. Materials & Methods.

3.1. Forestry data used for field validation.

Fieldwork was conducted approximately every two weeks between May 5th and September 27th 2022 (Table A). It focused on two sampling sites with differing geomorphic conditions : a site on the R2 reach where poplar trees were assumed to be well-connected to the river system (W+), and a site on the R1 reach where poplars were assumed to be disconnected from the

189 river and to have more limited access to groundwater (W-). Site selection was based on

190 previous work on the riparian forest by Dufour (2005) and Godfroy et al. (2023).

191 For each site, ten *Populus nigra* tree were selected, their diameter at breast height was

192 measured, and they were sampled during multiple campaigns at midday, near the solar zenith.

193

194 *3.1.2. Leaf water potential.*

195 For each campaign, two green leave shoots were collected for each of the trees and enclosed

196 in aluminium sheets to maintain dark conditions until measurements in the lab. Then, shoots

197 were kept in a cooling box for conservation before measuring leaf water potential (LWP)

198 using a pressure chamber once back at the laboratory (Scholander et al., 1965). The leaf petiol

199 was cut with a sharp blade and inserted in the pressure chamber. The mean pressure of the two

200 selected leaves per tree was used as, a single replicate.

201

202 *3.1.2. Phloem collection and iWUE calculation.*

203 Phloem of the trees was sampled every other field campaigns and used to estimate the

204 intrinsic water use efficiency (iWUE) of each tree according to the protocol published by

205 Gerle et al. (2023), based on relative ratios in carbon isotopes in the phloem content (Vernay

206 et al., 2020).

207 Briefly, phloem was collected with a bark-corer (9mm) at breast height in the trunk of each

208 tree and immersed in 1.5 mL exudation solution (15 mM polyphosphate buffer: sodium

209 hexametaphosphate, Sigma, München, Germany). Phloem was then removed from the tube

210 before freezing the solution. The samples were then freeze-dried and rehydrated with

211 deionised water in a tin capsule. After drying in a oven, the $^{13}C/^{12}C$ phloem ratio was analyzed

212 with a spectrometer and expressed in ‰ relative to Vienna Pee Dee Belemnite (VPDB).

213 Calculations to obtain iWUE are detailed in Gerle et al. (2023) and Vernay et al. (2020).

214

215 3.2. Remote-sensing data.

216 *3.2.1. Airborne TIR images.*

217 Images in the TIR spectrum (7.5–14 µm) were acquired in summer over four campaigns since

218 2010 [Table 2] with sensors mounted on an ultralight aircraft (2010 and 2022) or a helicopter

219 (2011 and 2014). Three different sensors were used: a Thermo Tracer TH7800 for the first

220 flight, a VarioCAM hr head for the second flight and a VarioCAM hr research 600 for the

221 third and fourth flights. These cameras can detect temperature differences of around 0.1°C

222 within an image. Days of flight were chosen based on the weather and during low-flow

223 conditions.

224 **Table 2 – Airborne TIR campaigns used in this study.**

Date	Time	Spatial resolution (m)	Mean daily discharge (m³.s-1)	Daily maximum temperature (°C)
July 30th 2010	15:00 to 16:00	1.50	14.3	25.6
June 28th 2011	17:45 to 18:30	0.70	13.4	34.0
July 3rd 2014	18:00 to 19:00	0.60	14.1	30.2
July 19th 2022	12:20 to 13:30	0.35	16.2	37.1

225

226 The images from the first three campaigns are historical TIR data available on the Ain River

227 that originally aimed at studying river temperature to identify the inter-annual variability of

228 cold-water patches. Therefore, the processing of these images is documented by the authors of

229 the initial study (Wawrzyniak et al., 2016). The last airborne campaign was coordinated with

230 the field campaign of this study (July 19th) and the flight took place during the same time-

231 frame.

232

233 *3.2.2. Satellite TIR images.*

234 Landsat satellites were used as a source of coarse historical TIR data starting from 1990 by

235 using level 2 images from Landsat 5, 8 and 9. Images from Landsat 7 were not considered for

236 the analysis due to the Scan Line Corrector failure that occurred in 2003. At most one image

237 was selected per year from the available data based on a rule of precipitation during the

238 summer period (a six-day window with no precipitation). This rule was defined according to

239 results from preliminary analysis of airborne TIR data that showed the difficulty of assessing

240 vegetation water stress from TIR imagery with wet antecedent conditions. This ensured that

241 selected images were from the driest possible period for every summer.

242

243 3.3. Additional information for geo-referencing, selecting and characterizing the study area.

244 Historical aerial photographs produced by the French Institut National de l'Information

245 Géographique et Forestière (IGN) were used to provide information about land cover for dates

246 close to the TIR campaigns. They were originally used by Wawrzyniak et al. (2016) to help

247 manually geo-reference the TIR images. Aerial color images were also acquired during the

248 2022 campaign by mounting a camera (Nikon Z6, 35 mm lens) on the aircraft during the TIR

249 acquisition and were similarly used to assess land cover in 2022 and to help with the geo-

250 referencing process.

251 Topo-bathymetric LiDAR data was acquired during August 2015 and covers the upstream half

252 of the study reach ($\approx$20 km), initially to study river bathymetry (Lague and Feldmann, 2020).

253 This dataset was then used to characterize the stationary conditions of the riparian forest in

13

254   Godfroy et al. (2023). It is used in this study to help assess the changes in canopy temperature

255   based on forest stationary conditions.

256   The data was acquired with an Optech Titan sensor flown on an airplane, and resulted in the

257   acquisition of a point cloud with a final density of around 18.6 points per meter square for

258   each of the two lasers of the sensor (Green for bathymetry and NIR for above-ground) and

259   with a mean vertical accuracy of ≈10 cm.

260   Vegetation surveys were conducted by ONF in 2007 and 2017 at the request of local

261   stakeholders. It led to the survey of *ca.* 1200 forest plots in the study reach with the goal of

262   providing extensive information on species distribution and health in the riparian forest of the

263   Ain River and, as such, one plot was assessed per hectare of forest. These vegetation plots

264   were used to provide an extensive analysis grid common to the forest surveys and to previous

265   studies (Godfroy et al., 2023) that covers the lower Ain River corridor. That grid is used for

266   selecting forest patches within which Landsat TIR information is analyzed.

267   Information about daily temperature and precipitations near the study site was accessed from

268   the open access archives of the Ambérieu-en-Bugey meteorological station available from the

269   Global Surface Summary of the Day (GSSD) provided by the National Centers for

270   Environmental Information (cf. https://www.ncei.noaa.gov/metadata/geoportal/). Information

271   on the flow level of the Ain River was measured at the hydrological station located at Pont

272   d'Ain and provided by the French Ministry of Ecological Transition (cf.

273   https://www.hydro.eaufrance.fr/).

274

275   3.4. General workflow.

276   Data analysis first focused on the campaign conducted during summer 2022 to investigate

277   how the water status of *Populus nigra* differed between the two study sites [Figure 2]. Water

278   status was assessed by monitoring changes in leaf water potential and intrinsic water use

279   efficiency from field samples. Differences in LWP or iWUE between poplars and between

280   sites were then assessed by running Student's test or Wilcoxon Mann-Whitney test depending

281   on data distribution for each date. Differences between each week were assessed by using a

282   pairwise t-test. Repeated measures ANOVA were then conducted to test the effects of

283   environment (W+ and W-) and time on LWP and iWUE values (environment, time and their

284   interaction were used as explanatory variables in the ANOVAs). Meteorological data from the

285   start of the campaign to its end were then plotted to recontextualize the observed trends in

286   water stress with the trends in air temperature and precipitations of summer 2022.
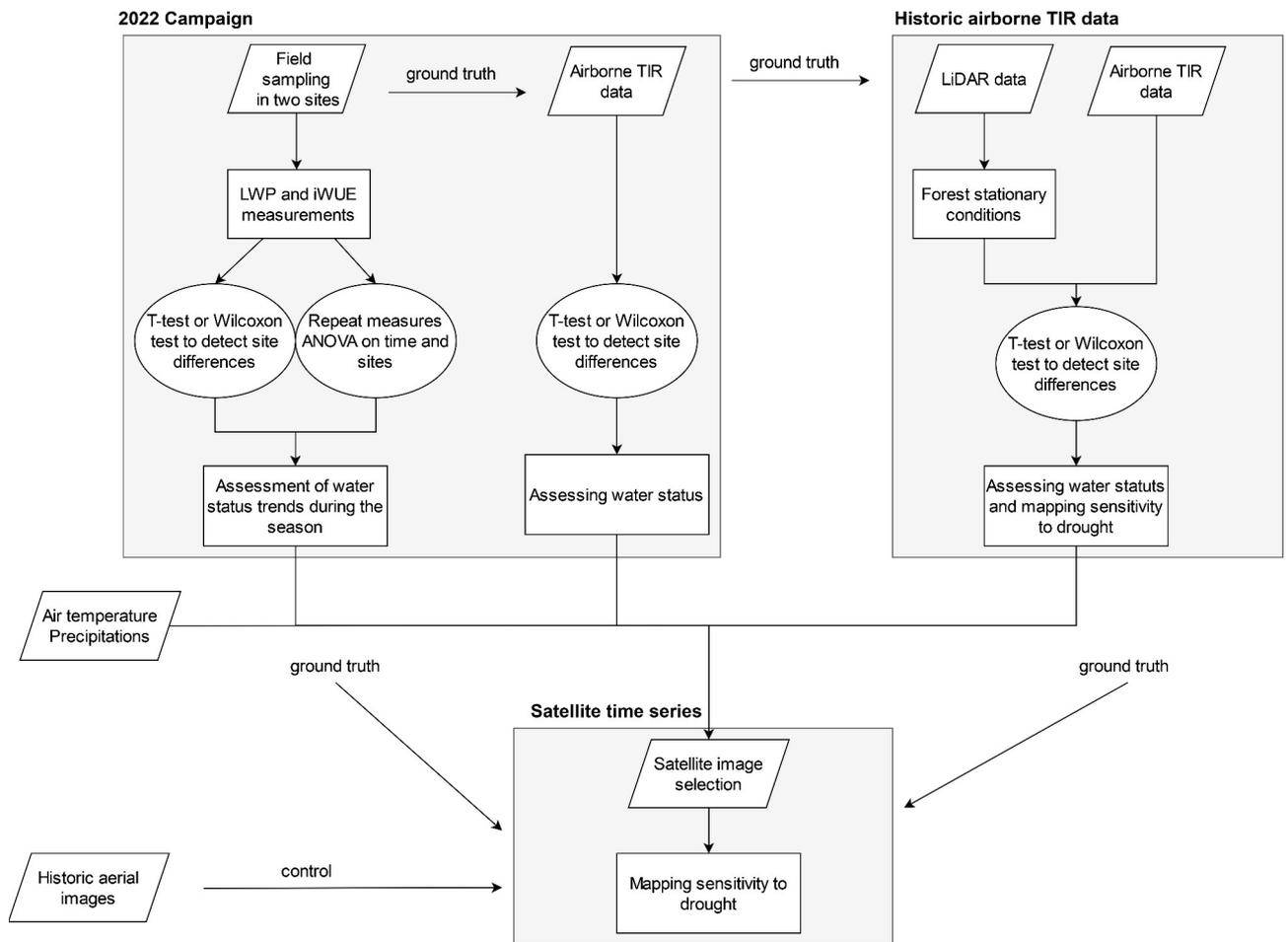
287

288   **Figure 2 – General workflow of our study.**

289   TIR data from 2022 was then analyzed by first looking at differences in tree crown

290   temperature between poplars from the two sites. In order to retrieve tree crown temperature,

291   the shape of each tree crown was first delineated manually by combining GPS positions of

292   each tree with the aerial images synchronous to the TIR acquisition and canopy height

293   extracted from the LiDAR dataset. Median temperature was then extracted for each tree

294   crown from TIR data. Differences between the poplars on the two sites were then assessed

295   using the same tests as for LWP and iWUE.

296   Tree diameter from the field survey and tree height from the LiDAR data were tested to

297   predict LWP, iWUE and TIR as potential variables to explain differences between individuals

298   on a given site for all dates during summer 2022 for which data was available.

299   Data analysis then focused on using existing airborne TIR imagery to detect water stress and

300   map the sensitivity of the riparian forest to drought. The relationship between canopy

301   temperature and stationary conditions at the level of forest plots was investigated for all four

302   campaigns.

303   In order to retrieve information on canopy temperature for each forestry plots, the closest

304   aerial images available to each campaign were used to screen forest plots and mask areas

305   which were not vegetated. The D90 of canopy temperatures was then extracted in each plot in

306   order to minimize effects from shadowing.

307   Stationary conditions were assessed by detrending LiDAR-derived DEM using the Fluvial

308   Corridor Toolbox (Roux et al., 2015). This detrended DEM was obtained by subtracting the

309   elevation of the water level of the river from the elevation of the terrestrial floodplain level,

310   resulting in values of elevation relative to the water level under low flow conditions ($Q = 16$

311    $m^3.s^{-1}$). The mean value from the detrended DEM was then extracted for all forest plots in the

312   coverage of the LiDAR data and used to create two classes of stationary conditions based on

313 previous literature on the Ain River (Dufour and Piégay, 2008; Godfroy et al., 2023), with a

314 "good connectivity" class for plots lower than 2.5 meters above low flow and a

315 "disconnected" class for plots 2.5 meters above low flow and higher.

316 The same methodology as for the analysis of the 2022 data was then applied by running

317 Student's test or Wilcoxon Mann-Whitney test depending on data distribution for each

318 campaign in order to detect differences in canopy temperature due to stationary conditions.

319 The campaign from 2022 was used as a control of the expected response in temperature

320 canopy under known stress conditions, and hydrological and meteorological data for the week

321 before the campaign were plotted to contextualize the observations.

322 Maps of riparian forest sensitivity to drought were then produced using relevant campaigns.

323 In order for maps to be comparable despite differences in atmospheric conditions at the time

324 of survey, canopy temperature values were discretized using quartile statistics.

325 Similar maps were then created using Landsat data to highlight lasting changes since 1990.

326 Image selection is described in the Satellite TIR images section of the manuscript. At-sensor

327 resolution (100–120 meters) was higher than the spatial footprint of the forest plots (20 meters

328 radius, with 100 meters between plot centers) so mean temperature was extracted for each plot

329 and a map was produced to help assess and discuss the impact of the original footprint of the

330 sensor on the results by using available orthophotos.

331

332 **4. Results.**

333 <u>4.1. Field validation of tree water stress and TIR response.</u>

334 Field surveys show that the water status of poplar trees varies during the summer period. In

335 particular, both sites reached stress conditions during summer since LWP values were

336 generally lower than -1.75 MPa from June to September [Figure 3a].

337
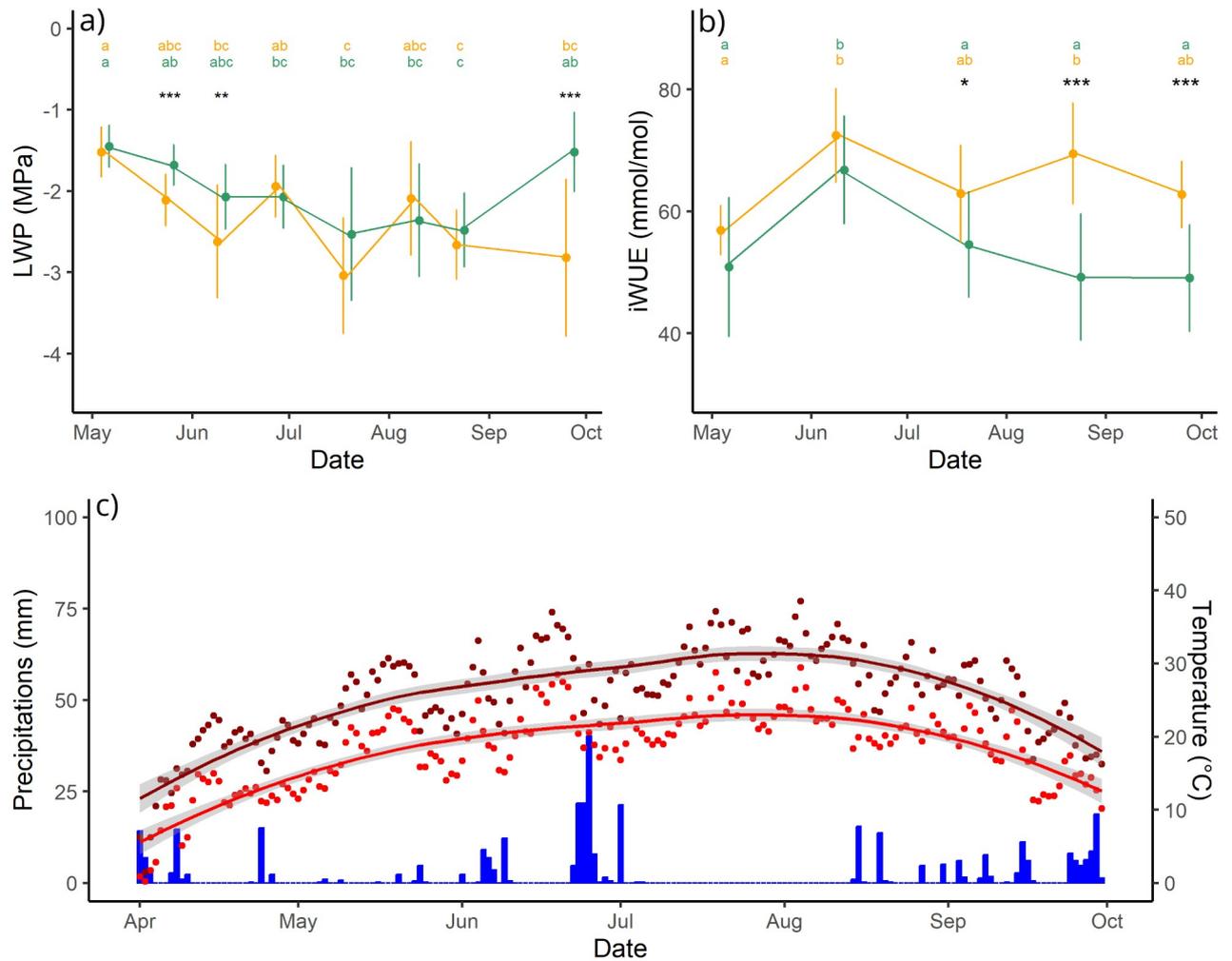
Figure 3. - (a) Leaf water potential (LWP) and (b) intrinsic water use efficiency (iWUE)
on the W+ site (green) and W- site (orange), and (c) precipitations (blue) and daily mean
(red) and daily maximum (dark red) temperatures for the study period. Stars indicate
differences in LWP or iWUE between the two sites (Wilcoxon or Student tests depending on data distribution, *
= p < 0.05, **= p < 0.001, *** = p < 0.001) and letters indicate the differences between dates from pairwise t
tests.

LWP values at the connected site (W+, in green) decreased until reaching a plateau near -2.5
MPa starting from the middle of June before increasing back to -1.5 MPa at the end of
September. For the disconnected site (W-, in orange), LWP decreased faster than for the
connected site, reaching values near -3 MPa on average in July. A more contrasted recovery is

18

348 observed for these poplars since LWP values at the end of September were still around -3

349 MPa on average, but variability between individuals increased which suggests partial

350 recovery. In addition, LWP values were more variable for poplars on the disconnected site

351 with short recovery periods (June 28th and August 9th) where mean LWP values were closer

352 to that of the connected site. Differences between sites were most significant at the beginning

353 of the stress period when LWP values increased with each subsequent campaign (May 25th

354 and June 10th) and at the end of September (September 26th) after which the connected site

355 fully benefits from the recovery period.

356 Although iWUE measurements were sparser and notably not conducted on June 28th or

357 August 9th (dates for which LWP values fluctuated for the disconnected site), they show a

358 trend similar to LWP measurements [Figure 3b]. An increase in iWUE values was observed

359 for both sites during summer, from 40–45 mmol/mol and reaching values near 50 mmol/mol

360 and 60 mmol/mol on average for the connected and disconnected sites respectively. A

361 recovery period is identified at the end of summer, with decreasing iWUE values starting

362 August 23rd for the connected site and at the end of September for the disconnected site.

363 While iWUE values were on average higher for poplars in the disconnected site, differences

364 between the two sites were significant during summer (July 19th and August 23rd) and at the

365 end of September.

366 The ANOVA tests performed on repeated measures indicated a significant effect of the

367 environment (W+ vs. W-, $p = 0.017$, $F = 8.583$), of the week of the sampling ($p < 10^{-3}$, $F =$

368 10.034) and of the environment × week interaction ($p < 10^{-3}$, $F = 4.413$) on LWP. For iWUE,

369 only an effect of the week ($p < 10^{-3}$, $F = 15.625$) and of the environment × week interaction (p

370 $< 10^{-3}$, $F = 3.412$) were significant, but not the effect of the environment alone ($p = 0.099$, $F =$

371 4.091).

372 Those two indicators converge towards an increasing water stress in *Populus nigra* during

373 summer and a recovery in late August or during September, which follows temperature and

374 rainfall trends for summer 2022 [Figure 3c].

375 Tree sampling and TIR data were acquired simultaneously on July 19th, which means all three

376 indicators of water stress can be compared for the disconnected (W-, in orange) and connected

377 (W+, in green) sites for the same date. On this date, LWP values were lower in the

378 disconnected site than in the connected site (Figure 4a), and the opposite was true for iWUE

379 values (Figure 4b). However these differences were only significant for iWUE (p < 0.05).

380 This validates a higher stress status in the disconnected site. Canopy temperature of sampled

381 trees was higher in the disconnected site (p < 0.05) which also suggests higher water stress for

382 poplars in the disconnected site (Figure 4c).
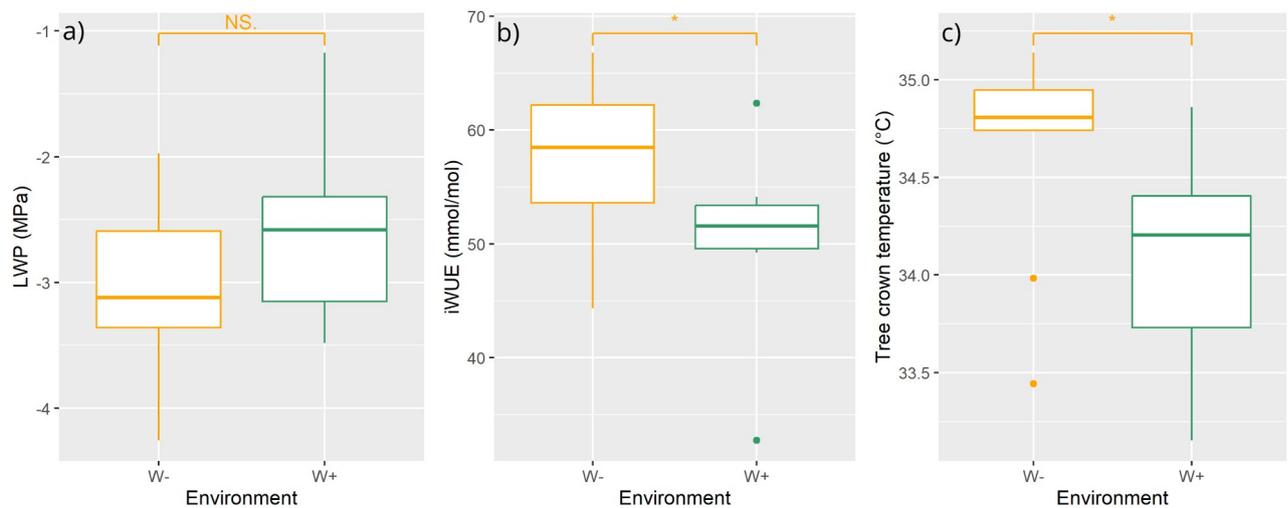
383

384 **Figure 4. - (a) Leaf water potential, (b) intrinsic water use efficiency and (c) tree crown**

385 **temperature depending on the study site on July 19th 2022.** Stars indicate differences between the

386 sites (Wilcoxon or Student tests depending on data distribution, * = p < 0.05, ** = p < 0.001, *** = p < 0.001).

387

388 The relationship between tree physiognomy and the three indicators of water stress was also

389 investigated (Figure 5). While r² values were low for most of the dates, intra-seasonal

20

390   variability was also recorded. Higher r² values were reached for LWP at the beginning of

391   summer for trees in the disconnected site (from 0.25 to 0.50) and for iWUE at the beginning

392   and the end of the summer for trees in the connected site (from 0.25 to 0.70). The relationship

393   between canopy temperature and tree height or tree diameter also reached high r² values for

394   the trees at the disconnected site (0.55 and 0.60 respectively). Overall, when a high r² value

395   was recorded, bigger trees (higher diameter or height) were less stressed (higher LWP, lower

396   iWUE and lower canopy temperatures) than smaller ones. Tree diameter was better correlated

397   than tree height for the disconnected site while the opposite was true for the connected site.
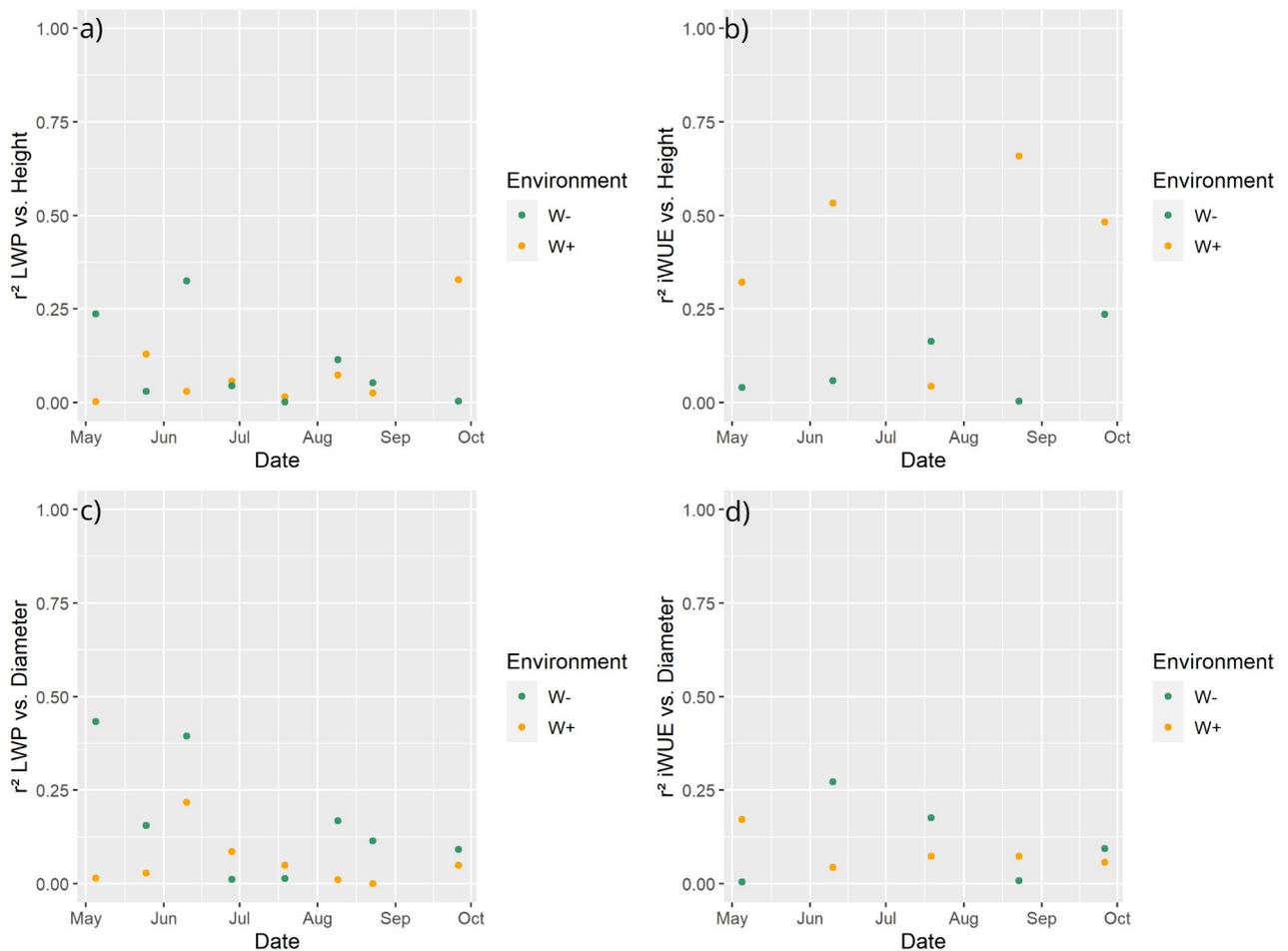

398

399   **Figure 5. - r² of the linear relationship between (a) LWP and tree height, (b) iWUE and**

400   **tree height, (c) LWP and tree diameter and (d) iWUE and tree diameter for each**

401   **sampling date and site.**

21

402

403 4.2. Inter-annual differences in airborne TIR response to summer conditions.

404 In the absence of *in-situ* assessment of the water status of the riparian forest for the historical

405 airborne surveys, only the thermal response of riparian vegetation to differences in

406 connectivity can be assessed. Using a breakpoint value of 2.5 meters above the low flow

407 water level as the main variable to consider shifts in connectivity, the results from an analysis

408 at the plot level in 2022 were similar to those of the analysis at the level of individual tree

409 crowns [Figure 6].
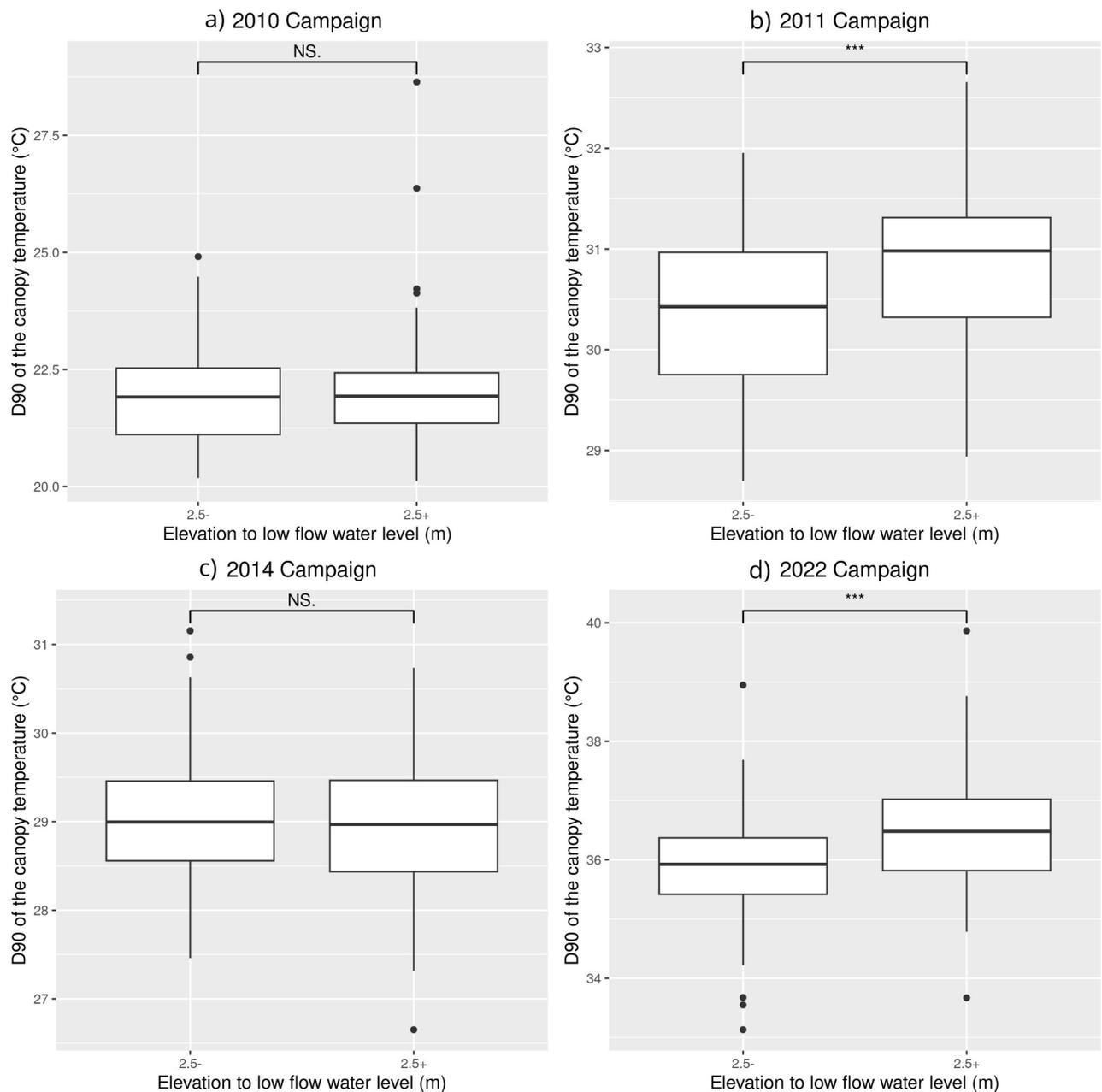
Figure 6. Canopy temperature at the plot level depending on plot elevation to low flow water level for all four airborne TIR campaigns: a) 2010, b) 2011, c) 2014 and d) 2022.

Stars indicate the differences between plots (results from Wilcoxon or Student tests depending on data

distribution * = p < 0.05, **= p < 0.001, *** = p < 0.001).

Indeed, in 2022 [Figure 6d] canopy temperature were higher for plots with higher elevation to the water table (p < 0.001) which is similar to the higher crown temperatures for trees in the disconnected site. While this was also true for the 2011 [Figure 6b] campaign (p-value <

418   0.001), there were no differences in canopy temperature between the two classes of stationary

419   conditions (connected for plots where elevation to low flow is < 2.5 meters and disconnected

420   for plots where it is > 2.5 meters) for 2010 [Figure 6a] and 2014 [Figure 6c]. Theses results

421   show temporal variability in the thermal response of riparian vegetation to its stationary

422   conditions.

423

424   4.3. Mapping of airborne TIR responses to summer droughts: 2011 vs. 2022.

425   The statistical distribution of canopy temperatures was mapped for 2011 and 2022 using

426   quartiles [Figure 7a], and a confrontation of the two maps (keeping only forest plots for which

427   thermal information was available in both 2011 and 2022) is shown [Figure 7b].

24

a)

R1

R2

R3

R4

b)

Quartiles of canopy
temperature

█ < Q1
█ [Q1, Q2]
█ [Q2, Q3]
█ > Q4

0   1   2 km

428

25
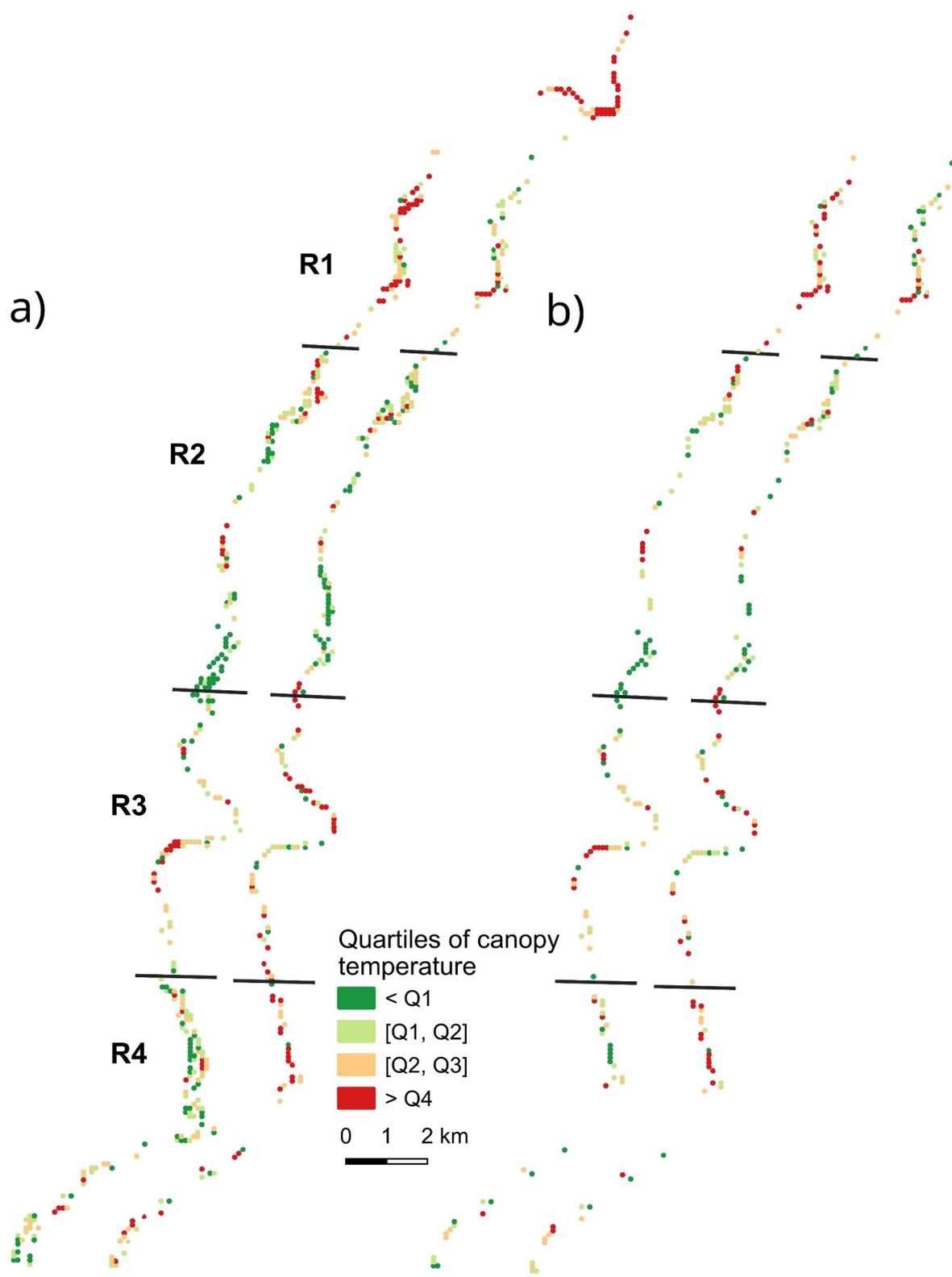
429   **Figure 7. - (a) Spatial distribution of the different quartiles of canopy temperature in**

430   **2011 and 2022 for all ONF plots, and (b) a 2011-2022 comparison using only plots for**

431   **which data was available both in 2011 and 2022.**
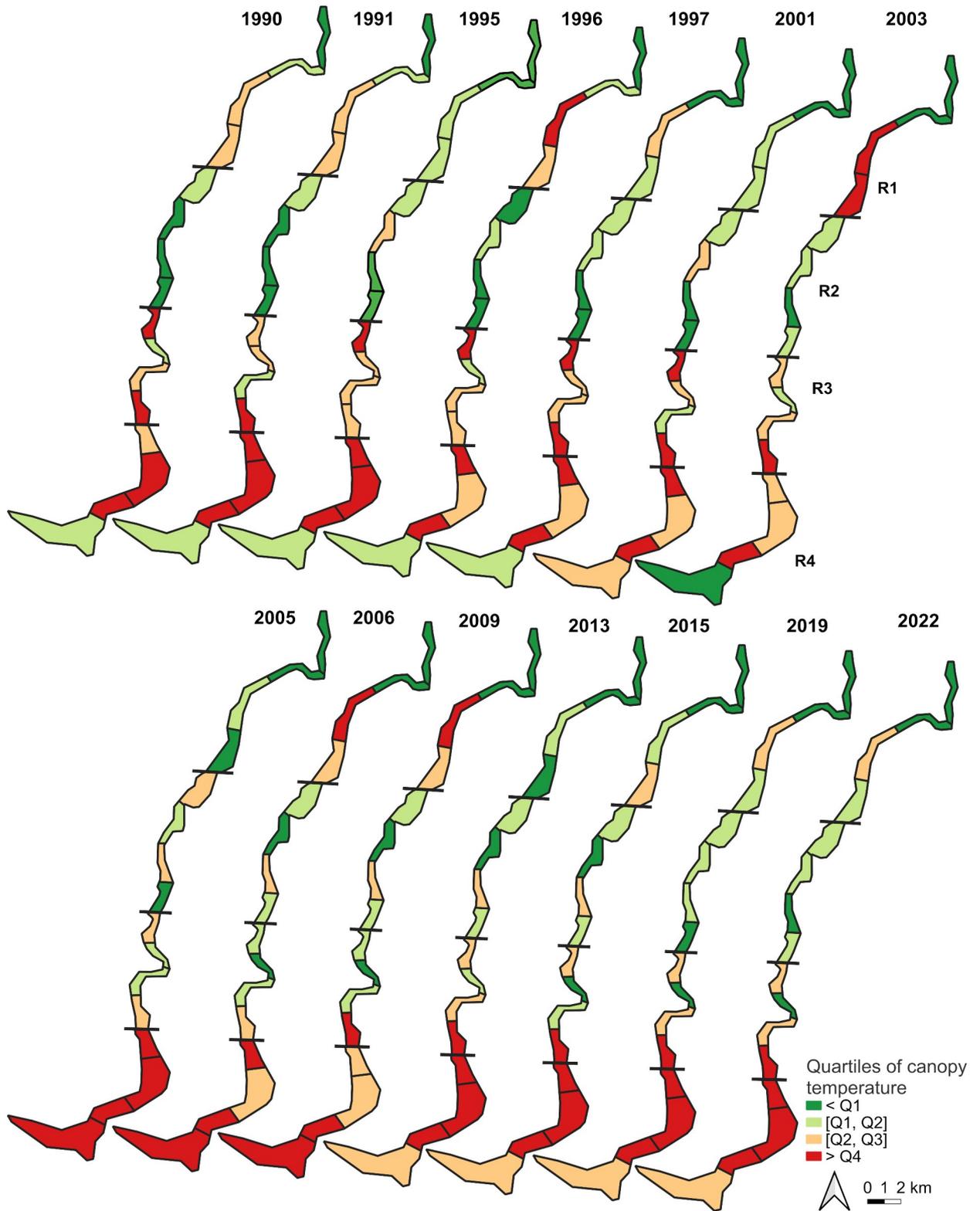
432   Both acquisitions covered most of the riparian corridor near the main channel of the Ain River

433   and poorly covered larger areas of riparian forest that were created by river meandering. The

434   higher canopy temperatures were concentrated in the R1 and R3 reaches, while the lower

435   canopy temperatures are located in the R2 and R4 reaches. As R1 was the most

436   geomorphologically-degraded reach suffering from historic channel incision and R2 was the

437   most geomorphologically-stable reach the spatial distribution of canopy temperature suggests

438   that the health of the riparian forest and its sensitivity to drought reflect 20th century changes

439   in geomorphology.

440   The distribution of canopy temperatures in 2022 was different from the one in 2011 with

441   lower quartiles of canopy temperature located in the R2 reach and higher quartiles being

442   located in the R3 and R4 reaches. Changes mainly occurred in the R1 and R4 reaches.

443

444   4.4. Mapping large-scale riparian thermal changes using Landsat archives.

445   Based on the results from field validation, selection of TIR Landsat data was constrained by

446   precipitation (no rain during a six-day period preceding observations from 2011 and 2022)

447   and by cloud cover (visually inspecting each image). With one image selected per year at a

448   maximum, this resulted in only 14 images selected for the 1990–2022 period. The resulting

449   maps also compared the distribution of temperature quartiles for each year but used all

450   available forest plots due to the higher spatial extent of satellite data [Figure 8].

26

1990 **1991** **1995** **1996** **1997** **2001** **2003**

R1

R2

R3

R4

2005 **2006** **2009** **2013** **2015** **2019** **2022**

Quartiles of canopy
temperature

< Q1
[Q1, Q2]
[Q2, Q3]
> Q4

0 1 2 km

451

452 **Figure 8. Spatial distribution of canopy temperature quartiles at the corridor scale from**

453 **Landsat data between 1990 and 2022.** Each reach was subdivided in four sectors of similar river length

454 and the information for each forest plot was summarized for each sector to facilitate reading.

455 The spatial distribution of canopy temperature quartiles was very similar for each year

456 satellite data was available. Plots showing higher temperature were mainly distributed in the

457 R1, R3 and R4 reaches, with most of the plots in the R2 reach being consistently among the

458 coolest plots. Lower temperatures also feature plots near the confluence with the Rhône River,

459 in the middle section of the R3 reach since the start of the new century, and plots near the

460 main channel or in the upstream-most section of reach R1.

461 Although the resolution of satellite thermal data is coarse, strong and meaningful change is

462 still highlighted in the area near the confluence with the Rhône River that is of interest to

463 understand forest dynamics in regards to meteorological and geomorphic constraints [Figure

464 9].
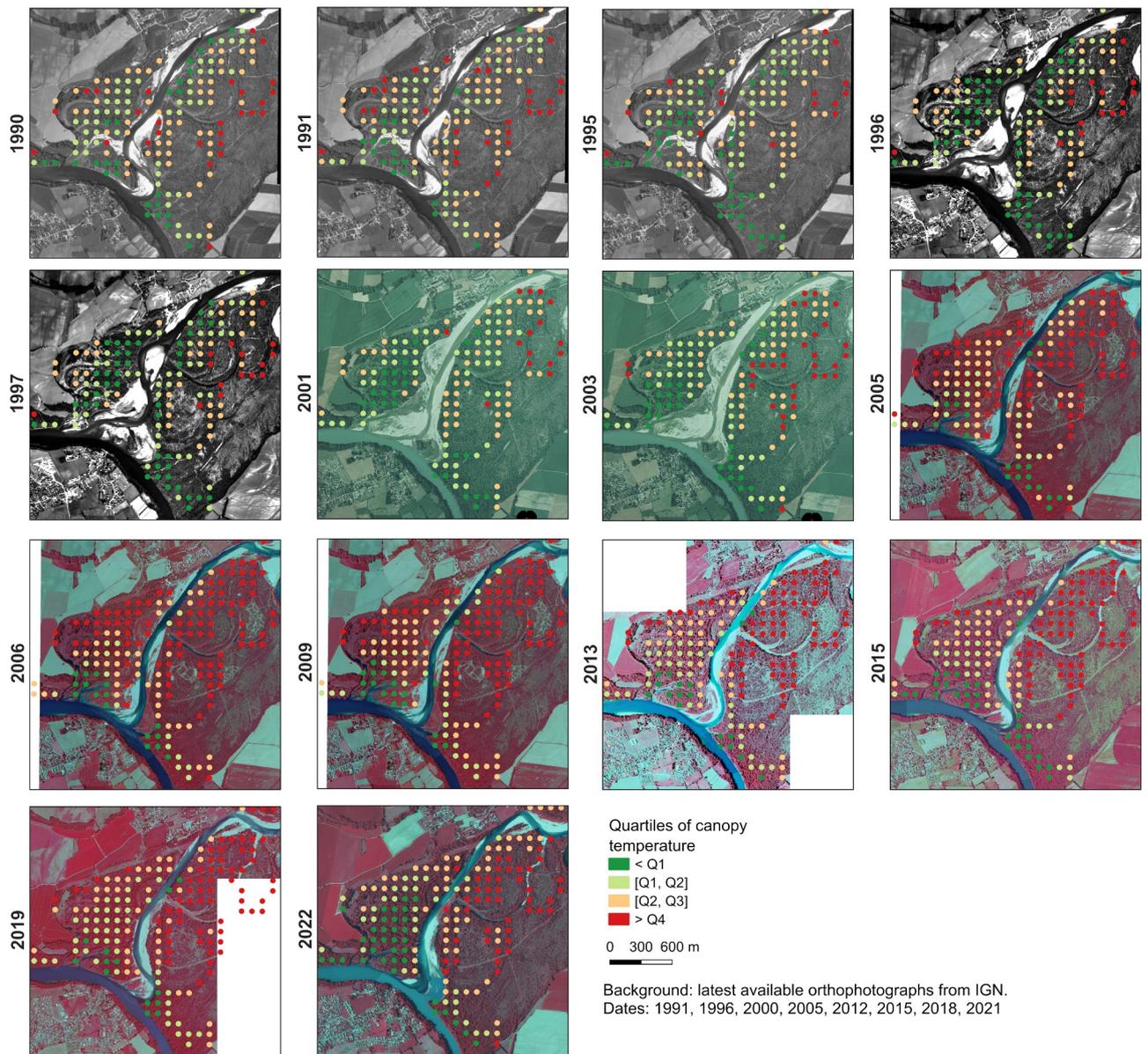
Figure 9. - Evolution of the sector at the confluence with the Rhône River since 1990.

On the aerial images, a simplification of channel morphology towards a lower active channel width is visible between 1995 and 2001 and illustrates the geomorphic changes that occurred at the end of the century in this section of the lower Ain River valley. In the case of the riparian forest, canopy temperature progressively increased relative to the rest of the lower Ain River valley between 2000 and 2005 leading to a shift from lower quartiles of

29

472   temperature to higher quartiles of temperature. This shift is more pronounced on the left side

473   of the river as the right side appears to have recovered by 2022.

474

475   **5. Discussion.**

476   <u>5.1. Summer water stress conditions of poplar trees depend on water accessibility.</u>

477   Our results suggest that the water stress conditions of riparian poplars depend on water

478   accessibility. Differences in the health status of trees were observed for all indicators (tree

479   crown temperature, LWP, iWUE), showing the contrasted response of *Populus nigra* to

480   drought based on its stationary conditions. The trees from the dryer site were consistently

481   showing higher water stress on one or more of the indicators used in this study, compared to

482   trees from the wetter site.

483   When considering a stress threshold at -1.75 MPa value for the leaf water potential, as

484   reported for *Populus nigra* stomatal closure in previous studies along the Drac and Isère rivers

485   (Lambs et al., 2006), stress conditions were reached for poplar individuals in summer 2022

486   regardless of their stationary conditions. While trees in more connected reaches of the river

487   were displaying lower stress according to the indicators (higher LWP, lower iWUE and lower

488   canopy temperature), they still experienced water scarcity. Therefore, the threat of drought-

489   induced changes in riparian forests can even affect river reaches with good geomorphic

490   conditions, and be exacerbated in river reaches where anthropogenic activity has already

491   historically altered water accessibility.

492   Such a change following a drought event was recorded in this study. Long-term change

493   analysis based on Landsat archives showed a shift in the riparian forest health status near the

494   confluence with the Rhône River. The timing of this change corresponds to the hottest and

495   driest summer recorded in France: the 2003 drought (Black et al., 2004; Luterbacher et al.,

496 2004). The fact that satellite data was able to detect such a change despite its coarse pixel

497 resolution suggests that the shift in forest structure is significant, with a more open canopy,

498 and a temperature measurement at sensor mixing the signals from the canopy, the understory

499 and potentially even the forest ground. This would be consistent with the field surveys by

500 ONF noticing a higher number of dead poplars in this sector and that they attributed to that

501 summer 2003 drought. Similar vegetation dieback has been recorded using remote sensing

502 data in other river systems following drought events (e.g. Kibler et al., 2021).

503 Tree response to stress however may vary. While tree mortality and the decline of the poplar

504 forest is one possible response to stress, it is not the only one. Water scarcity can also impact

505 tree growth and lead to changes in productivity of riparian trees (Lambs et al., 2006; Monclus

506 et al., 2006; Smith et al., 1991) and therefore impact both the ability of trees to act as carbon

507 sinks and their structure (*e.g.* diameter, height, leaf size). Specifically, for *Populus nigra*,

508 plasticity has been shown across a range of climatic conditions in Europe, with individuals

509 from certain locations (*e.g.* Spain) being more adapted to drier environments by having slower

510 growth with smaller leaves and a faster stomatal closure (Viger et al., 2016).

511 In our study, the relationships between tree height or diameter and several indicators were

512 tested but were only significant for a few dates. Trees on the disconnected site with a larger

513 diameter had higher LWP at the beginning of the stress period and lower canopy temperatures

514 during the TIR acquisition. On the other hand, trees from the connected site with a higher tree

515 height had a better recovery at the end of the summer. Interestingly, the allometric relationship

516 between tree height and tree diameter was distinct for the two sites (see Figure B). This

517 highlights how water scarcity, albeit due to channel incision (Godfroy et al., 2023; Rollet et

518 al., 2014), has already affected tree physiognomy in our study reach and may explain the

519 observed differences in tree response along the height – diameter gradient between sites.

520   Indeed, smaller trees are similar but differences in height-to-diameter ratios are observed

521   when trees grow larger.

522   In addition, not all historic airborne TIR data were collected under stressful conditions, as

523   only two campaigns showed changes in canopy temperature based on the vertical connectivity

524   of forest plot. Lower temperatures and higher precipitations before the two other campaigns

525   (Figure C) may not have led to stress conditions. Although our number of observations was

526   too low to be significant, the meteorological conditions in a three-day time period before the

527   campaign were strongly correlated to TIR-derived stress indicators (Figure D). This is also

528   supported by the intra-seasonal variability of the stress signal as measured by the LWP of the

529   poplar trees that showed a partial recovery for dates sampled following rainfall events.

530   This shows that identifying the role played by water accessibility in the response of riparian

531   forests to drought is difficult because it related to both river-related dynamics (such as access

532   to groundwater following channel incision or depending on flows during summer) and

533   meteorological dynamics (such as precipitations temporarily replenishing water content). In

534   addition, while we studied *Populus nigra* as it is a phreatophyte species, other species in the

535   riparian forest such as *Fraxinus excelsior* do not have the same root systems and are limited to

536   the vadose zone for accessing water resources (Dufour, 2005).

537

538   5.2. The benefits of a multi-tool approach to understand tree response to water stress.

539   Our results also shed light on the tools available to assess and monitor water stress in riparian

540   forests. One of our main findings in regards with the study design is that all our indicators

541   were sensitive to acquisition timing and did not always detect differences in stress intensity

542   based on forest stationary conditions, making it difficult to assess the stress status of the forest

543   or individual trees.

544 In-field sampling was used successfully to detect the occurence of water stress from May to

545 September and both LWP and iWUE showed an expected increase in stress intensity during

546 the summer. On the other hand, while both indicators detected differences between

547 individuals from the two sites, the dates for which results were the most significant did not

548 match except during the recovery period at the end of September.

549 Similarly, using airborne TIR data did not yield relevant results for all of the dates data was

550 available. Due to a lack of historic *in-situ* assessment of tree water status, it is not possible to

551 know if stress conditions would have been reported using another indicator. However, these

552 results show that the ideal acquisition window for studying vegetation health using thermal

553 data is not the same as the ideal acquisition window to study river temperature (*i.e.* the aim of

554 the initial historical study): data to study interactions between the river and groundwater

555 (Wawrzyniak et al., 2016) does not always provide accurate information on vegetation status.

556 However, it also means that having such wider implications in mind when planning data

557 collection can help optimise efforts and ressources in making data relavant beyond its original

558 use.

559 Considering ground truth, a careful study design based on antecedent hydro-climatic

560 conditions and a deep knowledge of geomorphic conditions in a river corridor seem crucial to

561 studies seeking to employ airborne TIR imagery to assess water stress.

562 However, some level of variability is to be expected since different indicators of water stress

563 do not correspond to the same biophysical processes and might not share the same response

564 time to environmental variables (Volaire, 2018), and water stress progresses from the upper

565 shoots in the tree crown to the tree trunk and the roots (Lambs et al., 2006).

566 For example, stomatal closure, which has been linked to changes in transpiration and an

567 increase in leaf temperature (Hsiao and Acevedo, 1974; Jones, 1999), occurs slowly over a

568　range of LWP depending on the rate of stress (Jones and Rawson, 1979). In *Populus nigra*,

569　higher rates of stomatal closure were related to higher iWUE (Viger et al., 2016). After

570　rewatering, the reopening of stomata lags behind recovery in LWP and the duration of this lag

571　is dependent on the degree of water stress and the species considered (Liang and Zhang,

572　1999). This is consistent with our observations of a delay between stress measured through

573　LWP and the increase in iWUE.

574　Overall, multi-tool monitoring would allow to better understand the stress signal of the

575　riparian forests in their natural conditions, and the delays between the responses that can be

576　measured at the canopy level with remote sensing and the events leading to stress conditions.

577　Additionally, using optical indexes or LiDAR data to retrieve parameters such as canopy

578　greenness and structure would also allow us to better understand under which conditions the

579　stress experienced by riparian trees leads to responses such as leaves yellowing, biomass loss,

580　and reduced growth.

581

582　5.3. Good practices in designing campaigns to monitor water stress in riparian ecosystems.

583　Based on this information and our results, designing campaigns to assess or monitor water

584　stress in riparian environment at large scales should couple TIR acquisitions with

585　complementary data to cross-validate the observations such as *in-situ* measurements of water

586　stress at target sites and optical remote-sensing indexes. Acquisitions would need to be

587　planned depending on when the stress is expected to occur, the lag in response for the

588　indicators used and their sensitivity to other environmental variables. Under these conditions,

589　multi-date surveys are recommended to obtain multiple observations for a given summer. Our

590　results also show that the acquisition of TIR data should target the peak of the stress period

34

591 and avoid dates with recent precipitations that could replenish water resources and affect air

592 humidity.

593 Another way to acquire TIR data would then be to rely on drones or satellites as other

594 airborne vectors such as helicopters or airplanes are less flexible in regards to the time of

595 acquisition and are more costly which limits both the ability to acquire data multiple times per

596 season and to target the most optimal window for TIR sensing of vegetation health. However,

597 the use of satellite TIR data is limited by the poor spatial resolution of current TIR sensor

598 which impacts their applicability to an early detection of water stress as they may be more

599 sensitive to more delayed responses to stress conditions such as changes in canopy structure

600 due to vegetation dieback and shifts in communities. Drone acquisitions suffer from lower

601 spatial extent but the technology is emerging for the study of river temperature (Dugdale et

602 al., 2022; Redana et al., 2024) after initial lowcost sensors proved prone to temperature

603 drifting (Dugdale et al., 2019). They would however provide the high temporal resolution

604 needed to better study how canopy temperature can be used as an indicator of water stress in

605 complex and heterogeneous riparian environments by coupling drone acquisitions with *in-situ*

606 surveys like those conducted in this study.

607 Multi-scale acquisition could help answer some of these issues by providing higher resolution

608 data as ground truth which is increasingly common when processing satellite data

609 (Carbonneau et al., 2020) or by using repeated drone surveys to help identify when more

610 costly airborne acquisitions over a larger spatial extent should be conducted.

611

612 5.4. Production of spatially-explicit knowledge for stakeholders and river management.

613 The results in this study builds upon previous research by validating the hypothesis that the

614 riparian forest of the Ain River experiences water stress in the summer. Previous studies

focused on an upstream–downstream gradient (Lejot et al., 2011) or on stationary conditions (Dufour, 2005; Godfroy et al., 2023; Rollet et al., 2014) to highlight differences in the health status of the riparian forest but did not directly approach water stress issues. Here, we were able to confirm the presence of water stress during the summer using ecophysiological *in-situ* measurement. We then discovered that water stress conditions impacted *Populus nigra* individuals in areas where we expected an unstressful water availability, shedding light on the fact that even better-connected sectors of the riparian forest were experiencing water stress during summer 2022.

By applying an approach previously known to have an impact on the growth of *Fraxinus excelsior* (Dufour, 2005) and on the distribution of species in the riparian forest and its structure (Godfroy et al., 2023), focused on stationary conditions, we also detected a direct effect of stationary conditions on the stress status of *Populus nigra*. Dryer stationary conditions due to channel incision led to higher levels of water stress during summer, and surveyed poplar trees experienced stress conditions earlier than those in reaches in better geomorphic conditions. These results support previous studies on other river systems that linked channel incision with an increase in mortality due to stress (Scott et al., 2000).

While *in-situ* assessments of the water status focused on *Populus nigra* because it was both the dominant species in the Ain River valley and of interest to local stakeholders, other riparian species might respond differently to droughts as previously described in section 5.1. This could limit results reproducibility and interpretability, yet in our study the relationship between forest stationary conditions and canopy temperature from airborne sensors held true at both the level of individual tree crowns and forest plots.

637 Overall, our results show that acquiring and using TIR data at various spatial scales can help

638 monitor the health status of riparian forests and their response to anthropic pressures to

639 generate actionable information for river managers.

640 In our case, we were able to detect a higher sensitivity of the riparian forest in Reach R4 to

641 the 2003 drought which may partly be explained by lower water access compared to Reach

642 R2 and by more pioneer populations compared to reaches R1 and R3. Since protecting

643 pioneer environments is one of the priorities of local stakeholders, our results indicate that

644 current gravel reinjection actions that focus on reaches R1 and R2 might not be sufficient to

645 protect riparian environments closer to the confluence with the Rhône River from drought. In

646 order to reduce the impact of climate change and warming weather on riparian forest, gravel

647 reinjections actions closer to this sector could be considered to limit channel straightening and

648 incision and improve groundwater access for pioneer trees. In a social context where the

649 construction of a dam on the Rhône River upstream the Ain–Rhône confluence is being

650 discussed, careful consideration needs to be given to the already fragilized riparian forest in

651 this sector as this could exacerbate water stress issues and contribute to a shift towards dryer

652 communities to the detriment of pioneer species such as *Populus nigra*.

653

654 **Conclusion.**

655 Water stress conditions were detected using *in-situ* measurements and showed increased water

656 stress on black poplars located in dryer terrestrial river margins. Airborne thermal infrared

657 remote sensing was able to detect this difference in water status due to an increase in canopy

658 temperature and enabled mapping of the riparian forest response to drought events on a 50 km

659 reach of the Ain River. Differences in the spatial distribution of forest sensitivity over a 10-

660 year period highlighted forest degradation in one of the reaches and provided feedback on

37

661   current restoration efforts. The use of satellite thermal infrared data was investigated but due

662   to coarse spatial resolution and the limited spatial extent of riparian corridors, observations

663   were more likely related to larger scale canopy openness and proximity to other land covers

664   rather than water status, therefore highlighting the need for further studies coupling satellite

665   data with ground truth acquired at higher resolution. Nonetheless, lasting degradations were

666   detected near the confluence of the Ain River with the Rhône River which can be attributed to

667   the combined effects of the 2003 drought event and groundwater levels lowering caused by

668   channel incision. However, the variation of the stress signal during summer and the fact that

669   not all surveys showed a temperature effect on tree canopy related to drought show the

670   importance of multi-date and multi-source surveys when attempting to assess or monitor

671   water stress in complex heterogeneous environments such as riparian forests. Despite these

672   requirements, airborne TIR mapping appears as a promising tool to monitor the response of

673   river systems to climate change thanks to its ability to inform about the water status of the

674   riparian forest and to additionally provide crucial information about other components of river

675   systems such as water surface temperature., but it needs to be repeated over the seasons and

676   years to detect long term effects of such potential ramp disturbance (e.g. cumulative effects of

677   heat pulses that are supposed to be more frequent and more intense).

678

695

696 **CRediT Statement.**

697 **J. Godfroy**: Conceptualization, Methodology, Formal Analysis, Investigation, Data Curation,

698 Writing - Original Draft, Writing – Review & Editing., **P. Malherbe**: Formal Analysis, Data

699 Curation, Writing – Review & Editing., **F. Gerle**: Formal Analysis, Data Curation, Writing –

700 Review & Editing., **B. Marteau**: Investigation, Methodology, Data Curation, Writing –

701 Review & Editing., **P. Lochin**: Investigation, Data Curation, Writing – Review & Editing., **S.**

702 **Puijalon**: Writing – Review & Editing, Supervision., **J. Lejot**: Writing – Review & Editing,

703 Supervision., **A. Vernay**: Conceptualization, Formal Analysis, Investigation, Data Curation,

704 Writing – Review & Editing, Supervision, Funding acquisition., **H. Piégay**:

705 Conceptualization, Methodology, Writing – Review & Editing, Supervision, Funding
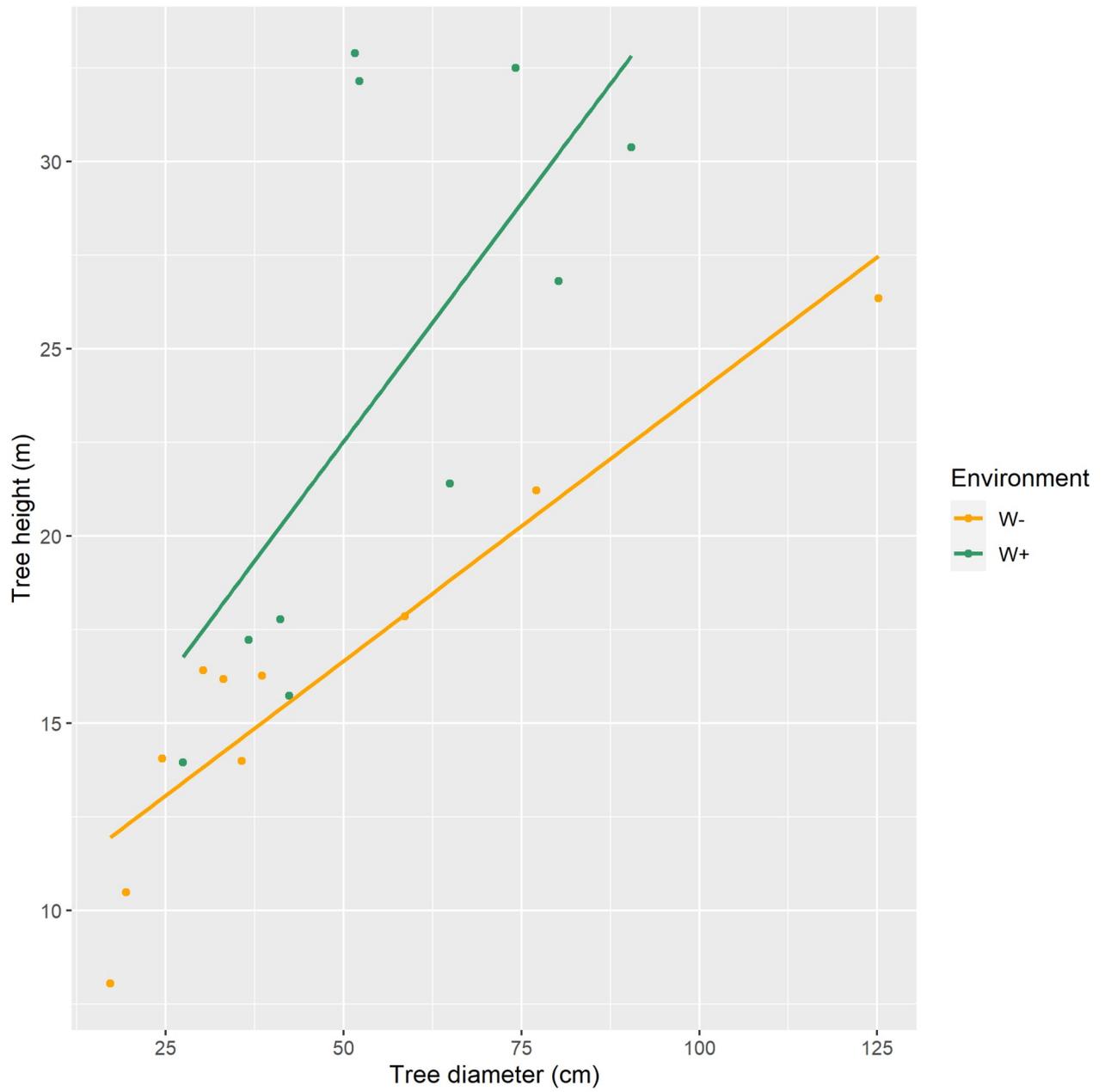
706 acquisition.

707 **Appendixes.**

708 <u>Table A. Dates for which leaf and phloem sampling was conducted during 2022.</u>

	Campaign Date							
	May 5th	May 25th	June 10th	June 28th	July 19th	Aug. 9th	Aug. 23rd	Sept. 27th
Leaf	X	X	X	X	X	X	X	X
Phloem	X		X		X		X	X

709

710

711 <u>Figure B. Relationship between tree height and tree diameter on the W+ site (r^2 = 0.47, p =</u>

712 <u>0.0285) and the W- site (r^2 = 0.85, p = 0.0001).</u>
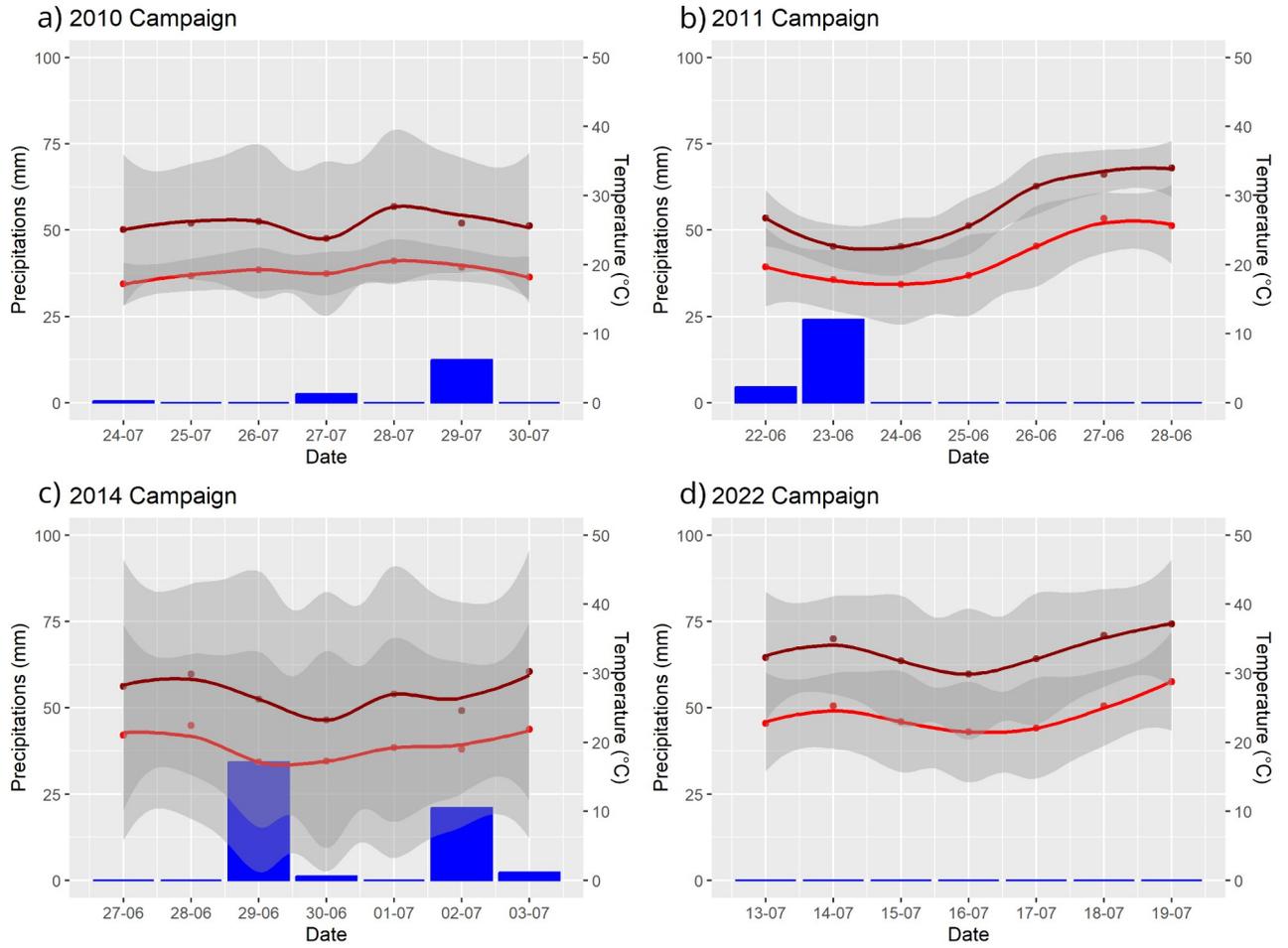

713

714

715

716 <u>Figure C. Precipitation (blue), daily mean (red) and daily maximum (dark red) temperatures</u>

717 <u>for a 7-day period preceding each airborne TIR campaign: a) 2010, b) 2011, c) 2014 and d)</u>

718 <u>2022.</u>

719

720

721 Figure D. Relationship between a) cumulative precipitations and b) mean maximum

722 temperature for a 3-day or 7-day time period and the observed difference in mean

723 temperatures from TIR data between the two elevation classes: connected (< 2.5 m from base

724 flow) and disconnected (> 2.5 m from base flow).
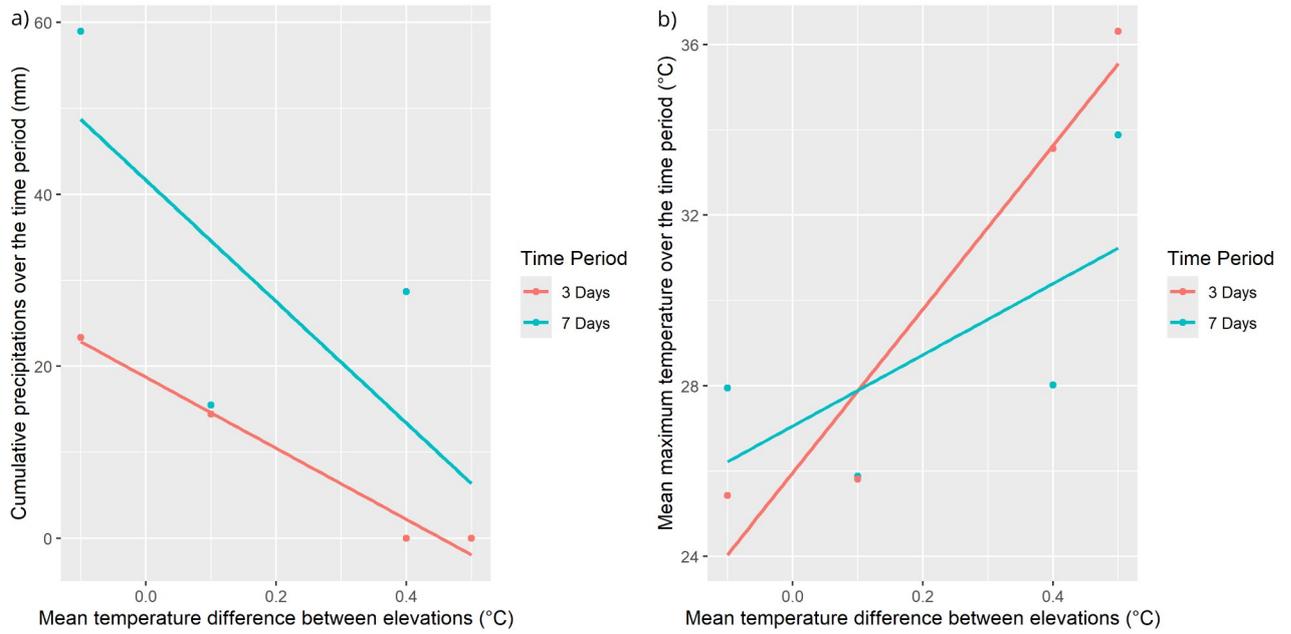
725

726 **Bibliography.**

Black, E., Blackburn, M., Harrison, G., Hoskins, B., Methven, J., 2004. Factors contributing to the summer 2003 European heatwave. Weather 59, 217–223. https://doi.org/10.1256/wea.74.04

Bravard, J.-P., Amoros, C., Pautou, G., Bornette, G., Bournaud, M., Creuzé des Châtelliers, M., Gibert, J., Peiry, J.-L., Perrin, J.-F., Tachet, H., 1997. River incision in south-east France: morphological phenomena and ecological effects. Regul. Rivers Res. Manag. 13, 75–90. https://doi.org/10.1002/(SICI)1099-1646(199701)13:1<75::AID-RRR444>3.0.CO;2-6

Breton, V., Girel, J., Janssen, P., 2023. Long-term changes in the riparian vegetation of a large, highly anthropized river: Towards less hygrophilous and more competitive communities. Ecol. Indic. 155, 111015. https://doi.org/10.1016/j.ecolind.2023.111015

Brodribb, T.J., Holbrook, N.M., 2003. Stomatal Closure during Leaf Dehydration, Correlation with Other Leaf Physiological Traits. Plant Physiol. 132, 2166–2173. https://doi.org/10.1104/pp.103.023879

Carbonneau, P.E., Belletti, B., Micotti, M., Lastoria, B., Casaioli, M., Mariani, S., Marchetti, G., Bizzi, S., 2020. UAV-based training for fully fuzzy classification of Sentinel-2 fluvial scenes. Earth Surf. Process. Landf. 45, 3120–3140. https://doi.org/10.1002/esp.4955

Ciężkowski, W., Kleniewska, M., Chormański, J., 2020. Thermal and Optical Indices for Wetland Habitats, are They Showing the Same Thing? IEEE J. Sel. Top. Appl. Earth Obs. Remote Sens. 13, 3951–3957. https://doi.org/10.1109/JSTARS.2020.3008864

Comiti, F., Da Canal, M., Surian, N., Mao, L., Picco, L., Lenzi, M.A., 2011. Channel adjustments and vegetation cover dynamics in a large gravel bed river over the last 200years. Geomorphology 125, 147–159. https://doi.org/10.1016/j.geomorph.2010.09.011

Décamps, H., Fortuné, M., Gazelle, F., Pautou, G., 1988. Historical influence of man on the riparian dynamics of a fluvial landscape. Landsc. Ecol. 1, 163–173. https://doi.org/10.1007/BF00162742

Dépret, T., Thommeret, N., Piégay, H., Gautier, E., 2023. Can lateral mobility be restored along a highly domesticated low-energy gravel-bed river? J. Environ. Manage. 325, 116485. https://doi.org/10.1016/j.jenvman.2022.116485

Dosskey, M.G., Vidon, P., Gurwick, N.P., Allan, C.J., Duval, T.P., Lowrance, R., 2010. The Role of Riparian Vegetation in Protecting and Improving Chemical Water Quality in Streams1. JAWRA J. Am. Water Resour. Assoc. 46, 261–277. https://doi.org/10.1111/j.1752-1688.2010.00419.x

Dufour, S., 2005. Contrôles naturels anthropiques de la structure et de la dynamique des forêts riveraines (PhD Thesis). Université Jean Moulin Lyon III, Lyon.

Dufour, S., Piégay, H., 2008. Geomorphological Controls of Fraxinus Excelsior Growth and Regeneration in Floodplain Forests. Ecology 89, 205–215. https://doi.org/10.1890/06-1768.1

Dugdale, S.J., 2016. A practitioner's guide to thermal infrared remote sensing of rivers and streams: recent advances, precautions and considerations. WIREs Water 3, 251–268. https://doi.org/10.1002/wat2.1135

Dugdale, S.J., Franssen, J., Corey, E., Bergeron, N.E., Lapointe, M., Cunjak, R.A., 2016. Main stem movement of Atlantic salmon parr in response to high river temperature. Ecol. Freshw. Fish 25, 429–445. https://doi.org/10.1111/eff.12224

Dugdale, S.J., Kelleher, C.A., Malcolm, I.A., Caldwell, S., Hannah, D.M., 2019. Assessing the potential of drone-based thermal infrared imagery for quantifying river temperature heterogeneity. Hydrol. Process. 33, 1152–1163. https://doi.org/10.1002/hyp.13395

Dugdale, S.J., Klaus, J., Hannah, D.M., 2022. Looking to the Skies: Realising the Combined Potential of Drones and Thermal Infrared Imagery to Advance Hydrological Process Understanding in Headwaters. Water Resour. Res. 58, e2021WR031168. https://doi.org/10.1029/2021WR031168

Dugdale, S.J., Malcolm, I.A., Kantola, K., Hannah, D.M., 2018. Stream temperature under contrasting riparian forest cover: Understanding thermal dynamics and heat exchange processes. Sci. Total Environ. 610–611, 1375–1389. https://doi.org/10.1016/j.scitotenv.2017.08.198

Dumas, S., 2017. Inventaire des boisements forestiers de la Basse Vallée de l'Ain. Office National des Forêts.

Dumas, S., Perrin, V., 2006. Le suivi de la forêt alluviale de la Basse Vallée de l'Ain : Inventaire de niveau II de 2006. Office National des Forêts.

Fairfax, E., Small, E.E., 2018. Using remote sensing to assess the impact of beaver damming on riparian evapotranspiration in an arid landscape. Ecohydrology 11, e1993. https://doi.org/10.1002/eco.1993

Gerle, F., Malherbe, P., Boisselet, C., Lafleuriel, D., Godfroy, J., Lochin, P., Marteau, B., Piegay, H., Puijalon, S., Vernay, A., 2023. Intrinsic water use efficiency estimate: an isotopic method.

Godfroy, J., Lejot, J., Demarchi, L., Bizzi, S., Michel, K., Piégay, H., 2023. Combining Hyperspectral, LiDAR, and Forestry Data to Characterize Riparian Forests along Age and Hydrological Gradients. Remote Sens. 15, 17. https://doi.org/10.3390/rs15010017

Gokool, S., Jarmain, C., Riddell, E., Swemmer, A., Lerm, R., Chetty, K.T., 2017. Quantifying riparian total evaporation along the Groot Letaba River: A comparison between infilled and

spatially downscaled satellite derived total evaporation estimates. J. Arid Environ. 147, 114–124. https://doi.org/10.1016/j.jaridenv.2017.07.014

González del Tánago, M., Martínez-Fernández, V., Aguiar, F.C., Bertoldi, W., Dufour, S., García de Jalón, D., Garófano-Gómez, V., Mandzukovski, D., Rodríguez-González, P.M., 2021. Improving river hydromorphological assessment through better integration of riparian vegetation: Scientific evidence and guidelines. J. Environ. Manage. 292, 112730. https://doi.org/10.1016/j.jenvman.2021.112730

Hsiao, T.C., Acevedo, E., 1974. Plant responses to water deficits, water-use efficiency, and drought resistance. Agric. Meteorol., Plant modification for more efficient water use 14, 59–84. https://doi.org/10.1016/0002-1571(74)90011-9

Janssen, P., Stella, J.C., Piégay, H., Räpple, B., Pont, B., Faton, J.-M., Cornelissen, J.H.C., Evette, A., 2020. Divergence of riparian forest composition and functional traits from natural succession along a degraded river with multiple stressor legacies. Sci. Total Environ. 721, 137730. https://doi.org/10.1016/j.scitotenv.2020.137730

Jones, H.G., 1999. Use of infrared thermometry for estimation of stomatal conductance as a possible aid to irrigation scheduling. Agric. For. Meteorol. 95, 139–149. https://doi.org/10.1016/S0168-1923(99)00030-1

Jones, M.M., Rawson, H.M., 1979. Influence of Rate of Development of Leaf Water Deficits upon Photosynthesis, Leaf Conductance, Water Use Efficiency, and Osmotic Potential in Sorghum. Physiol. Plant. 45, 103–111. https://doi.org/10.1111/j.1399-3054.1979.tb01672.x

Kibler, C.L., Schmidt, E.C., Roberts, D.A., Stella, J.C., Kui, L., Lambert, A.M., Singer, M.B., 2021. A brown wave of riparian woodland mortality following groundwater declines during the 2012–2019 California drought. Environ. Res. Lett. 16, 084030. https://doi.org/10.1088/1748-9326/ac1377

Klein, T., Rotenberg, E., Tatarinov, F., Yakir, D., 2016. Association between sap flow-derived and eddy covariance-derived measurements of forest canopy CO_2 uptake. New Phytol. 209, 436–446. https://doi.org/10.1111/nph.13597

Lague, D., Feldmann, B., 2020. Topo-bathymetric airborne LiDAR for fluvial-geomorphology analysis, in: Paolo Tarolli, S.M.M. (Eds.) (Ed.), Remote Sensing of Geomorphology, Developments in Earth Surface Processes. Elsevier, pp. 25–54. https://doi.org/10.1016/B978-0-444-64177-9.00002-3

Lambs, L., Loubiat, M., Girel, J., Tissier, J., Peltier, J.-P., Marigo, G., 2006. Survival and acclimatation of Populus nigra to drier conditions after damming of an alpine river, southeast France. Ann. For. Sci. 63, 377–385. https://doi.org/10.1051/forest:2006018

Lejot, J., Piégay, H., Hunter, P.D., Moulin, B., Gagnage, M., 2011. Utilisation de la télédétection pour la caractérisation des corridors fluviaux : exemples d'applications et enjeux actuels. Géomorphologie Relief Process. Environ. 17, 157–172. https://doi.org/10.4000/geomorphologie.9362

Liang, J., Zhang, J., 1999. The relations of stomatal closure and reopening to xylem ABA concentration and leaf water potential during soil drying and rewatering. Plant Growth Regul. 29, 77–86. https://doi.org/10.1023/A:1006207900619

Lurtz, M.R., Morrison, R.R., Gates, T.K., Senay, G.B., Bhaskar, A.S., Ketchum, D.G., 2020. Relationships between riparian evapotranspiration and groundwater depth along a semiarid irrigated river valley. Hydrol. Process. 34, 1714–1727. https://doi.org/10.1002/hyp.13712

Luterbacher, J., Dietrich, D., Xoplaki, E., Grosjean, M., Wanner, H., 2004. European Seasonal and Annual Temperature Variability, Trends, and Extremes Since 1500. Science 303, 1499–1503. https://doi.org/10.1126/science.1093877

Marteau, B., Michel, K., Piégay, H., 2022a. Can gravel augmentation restore thermal functions in gravel-bed rivers? A need to assess success within a trajectory-based before–after control–impact framework. Hydrol. Process. 36, e14480. https://doi.org/10.1002/hyp.14480

Marteau, B., Piégay, H., Chandesris, A., Michel, K., Vaudor, L., 2022b. Riparian shading mitigates warming but cannot revert thermal alteration by impoundments in lowland rivers. Earth Surf. Process. Landf. n/a. https://doi.org/10.1002/esp.5372

Mayes, M., Caylor, K.K., Singer, M.B., Stella, J.C., Roberts, D., Nagler, P., 2020. Climate sensitivity of water use by riparian woodlands at landscape scales. Hydrol. Process. 34, 4884–4903. https://doi.org/10.1002/hyp.13942

Monclus, R., Dreyer, E., Villar, M., Delmotte, F.M., Delay, D., Petit, J.-M., Barbaroux, C., Le Thiec, D., Bréchet, C., Brignolas, F., 2006. Impact of drought on productivity and water use efficiency in 29 genotypes of Populus deltoides×Populus nigra. New Phytol. 169, 765–777. https://doi.org/10.1111/j.1469-8137.2005.01630.x

Naiman, R., J., Decamps, H., Pastor, J., Johnston, C., 1988. The Potential Importance of Boundaries to Fluvial Ecosystems. J. North Am. Benthol. Soc. 7. https://doi.org/10.2307/1467295

Naiman, R.J., Decamps, H., Pollock, M., 1993. The Role of Riparian Corridors in Maintaining Regional Biodiversity. Ecol. Appl. Publ. Ecol. Soc. Am. 3, 209–212. https://doi.org/10.2307/1941822

Neale, C.M.U., Geli, H., Taghvaeian, S., Masih, A., Pack, R.T., Simms, R.D., Baker, M., Milliken, J.A., O'Meara, S., Witherall, A.J., 2011. Estimating evapotranspiration of riparian vegetation using high resolution multispectral, thermal infrared and lidar data, in: Remote Sensing for Agriculture, Ecosystems, and Hydrology XIII. SPIE, pp. 254–262. https://doi.org/10.1117/12.903246

O'Briain, R., 2019. Climate change and European rivers: An eco-hydromorphological perspective. Ecohydrology 12, e2099. https://doi.org/10.1002/eco.2099

Poff, N.L., Olden, J.D., Merritt, D.M., Pepin, D.M., 2007. Homogenization of regional river dynamics by dams and global biodiversity implications. Proc. Natl. Acad. Sci. 104, 5732–5737. https://doi.org/10.1073/pnas.0609812104

Redana, M., Lancaster, L.T., Chong, X.Y., Lip, Y.Y., Gibbins, C., 2024. An open-source method for producing reliable water temperature maps for ecological applications using non-radiometric sensors. Remote Sens. Appl. Soc. Environ. 34, 101184. https://doi.org/10.1016/j.rsase.2024.101184

Riis, T., Kelly-Quinn, M., Aguiar, F.C., Manolaki, P., Bruno, D., Bejarano, M.D., Clerici, N., Fernandes, M.R., Franco, J.C., Pettit, N., Portela, A.P., Tammeorg, O., Tammeorg, P., Rodríguez-González, P.M., Dufour, S., 2020. Global Overview of Ecosystem Services Provided by Riparian Vegetation. BioScience 70, 501–514. https://doi.org/10.1093/biosci/biaa041

Rivaes, R., Rodríguez-González, P.M., Albuquerque, A., Pinheiro, A.N., Egger, G., Ferreira, M.T., 2013. Riparian vegetation responses to altered flow regimes driven by climate change in Mediterranean rivers. Ecohydrology 6, 413–424. https://doi.org/10.1002/eco.1287

Rohde, M.M., Stella, J.C., Roberts, D.A., Singer, M.B., 2021. Groundwater dependence of riparian woodlands and the disrupting effect of anthropogenically altered streamflow. Proc. Natl. Acad. Sci. 118, e2026453118. https://doi.org/10.1073/pnas.2026453118

Rollet, A.J., 2007. Etude et gestion de la dynamique sédimentaire d'un tronçon fluvial à l'aval d'un barrage : le cas de la basse vallée de l'Ain (PhD Thesis). Université Jean Moulin Lyon 3.

Rollet, A.J., Piégay, H., Dufour, S., Bornette, G., Persat, H., 2014. Assessment of Consequences of Sediment Deficit on a Gravel River Bed Downstream of Dams in

Restoration Perspectives: Application of a Multicriteria, Hierarchical and Spatially Explicit Diagnosis. River Res. Appl. 30, 939–953. https://doi.org/10.1002/rra.2689

Roux, C., Alber, A., Bertrand, M., Vaudor, L., Piégay, H., 2015. "FluvialCorridor": A new ArcGIS toolbox package for multiscale riverscape exploration. Geomorphology, Geomorphology in the Geocomputing Landscape: GIS, DEMs, Spatial Analysis and statistics 242, 29–37. https://doi.org/10.1016/j.geomorph.2014.04.018

Sankey, T., Hultine, K., Blasini, D., Koepke, D., Bransky, N., Grady, K., Cooper, H., Gehring, C., Allan, G., 2021. UAV thermal image detects genetic trait differences among populations and genotypes of Fremont cottonwood (Populus fremontii, Salicaceae). Remote Sens. Ecol. Conserv. 7, 245–258. https://doi.org/10.1002/rse2.185

Scholander, P.F., Bradstreet, E.D., Hemmingsen, E.A., Hammel, H.T., 1965. Sap Pressure in Vascular Plants. Science 148, 339–346. https://doi.org/10.1126/science.148.3668.339

Scott, M.L., Lines, G.C., Auble, G.T., 2000. Channel incision and patterns of cottonwood stress and mortality along the Mojave River, California. J. Arid Environ. 44, 399–414. https://doi.org/10.1006/jare.1999.0614

Seibt, U., Rajabi, A., Griffiths, H., Berry, J.A., 2008. Carbon isotopes and water use efficiency: sense and sensitivity. Oecologia 155, 441–454. https://doi.org/10.1007/s00442-007-0932-7

Simon, A., Collison, A.J.C., 2002. Quantifying the mechanical and hydrologic effects of riparian vegetation on streambank stability. Earth Surf. Process. Landf. 27, 527–546. https://doi.org/10.1002/esp.325

Singer, M.B., Stella, J.C., Dufour, S., Piégay, H., Wilson, R.J.S., Johnstone, L., 2013. Contrasting water-uptake and growth responses to drought in co-occurring riparian tree species. Ecohydrology 6, 402–412. https://doi.org/10.1002/eco.1283

Smith, S.D., Wellington, A.B., Nachlinger, J.L., Fox, C.A., 1991. Functional Responses of Riparian Vegetation to Streamflow Diversion in the Eastern Sierra Nevada. Ecol. Appl. 1, 89–97. https://doi.org/10.2307/1941850

Stella, J.C., Riddle, J., Piégay, H., Gagnage, M., Trémélo, M.-L., 2013a. Climate and local geomorphic interactions drive patterns of riparian forest decline along a Mediterranean Basin river. Geomorphology, Process geomorphology and ecosystems: Disturbance regimes and interactions 202, 101–114. https://doi.org/10.1016/j.geomorph.2013.01.013

Stella, J.C., Rodríguez-González, P.M., Dufour, S., Bendix, J., 2013b. Riparian vegetation research in Mediterranean-climate regions: common patterns, ecological processes, and considerations for management. Hydrobiologia 719, 291–315. https://doi.org/10.1007/s10750-012-1304-9

Tabacchi, E., Lambs, L., Guilloy, H., Planty-Tabacchi, A.-M., Muller, E., Décamps, H., 2000. Impacts of riparian vegetation on hydrological processes. Hydrol. Process. 14, 2959–2976. https://doi.org/10.1002/1099-1085(200011/12)14:16/17<2959::AID-HYP129>3.0.CO;2-B

Vernay, A., Tian, X., Chi, J., Linder, S., Mäkelä, A., Oren, R., Peichl, M., Stangl, Z.R., Tor-Ngern, P., Marshall, J.D., 2020. Estimating canopy gross primary production by combining phloem stable isotopes with canopy and mesophyll conductances. Plant Cell Environ. https://doi.org/10.1111/pce.13835

Viger, M., Smith, H.K., Cohen, D., Dewoody, J., Trewin, H., Steenackers, M., Bastien, C., Taylor, G., 2016. Adaptive mechanisms and genomic plasticity for drought tolerance identified in European black poplar (Populus nigra L.). Tree Physiol. 36, 909–928. https://doi.org/10.1093/treephys/tpw017

Volaire, F., 2018. A unified framework of plant adaptive strategies to drought: Crossing scales and disciplines. Glob. Change Biol. 24, 2929–2938. https://doi.org/10.1111/gcb.14062

Wawrzyniak, V., Allemand, P., Bailly, S., Lejot, J., Piégay, H., 2017. Coupling LiDAR and thermal imagery to model the effects of riparian vegetation shade and groundwater inputs on summer river temperature. Sci. Total Environ. 592, 616–626. https://doi.org/10.1016/j.scitotenv.2017.03.019

Wawrzyniak, V., Piégay, H., Allemand, P., Vaudor, L., Goma, R., Grandjean, P., 2016. Effects of geomorphology and groundwater level on the spatio-temporal variability of riverine cold water patches assessed using thermal infrared (TIR) remote sensing. Remote Sens. Environ. 175, 337–348. https://doi.org/10.1016/j.rse.2015.12.050

Whitledge, G.W., Rabeni, C.F., Annis, G., Sowa, S.P., 2006. Riparian Shading and Groundwater Enhance Growth Potential for Smallmouth Bass in Ozark Streams. Ecol. Appl. 16, 1461–1473. https://doi.org/10.1890/1051-0761(2006)016[1461:RSAGEG]2.0.CO;2

Wilbur, N.M., O'Sullivan, A.M., MacQuarrie, K.T.B., Linnansaari, T., Curry, R.A., 2020. Characterizing physical habitat preferences and thermal refuge occupancy of brook trout (Salvelinus fontinalis) and Atlantic salmon (Salmo salar) at high river temperatures. River Res. Appl. 36, 769–783. https://doi.org/10.1002/rra.3570

727